

AperTO - Archivio Istituzionale Open Access dell'Università di Torino

**Design of active debris flow mitigation measures: a comprehensive analysis of existing impact models**

**This is the author's manuscript**

*Original Citation:*

*Availability:*

This version is available <http://hdl.handle.net/2318/1711799> since 2019-11-14T08:36:46Z

*Published version:*

DOI:10.1007/s10346-019-01278-5

*Terms of use:*

Open Access

Anyone can freely access the full text of works made available as "Open Access". Works made available under a Creative Commons license can be used according to the terms and conditions of said license. Use of all other works requires consent of the right holder (author or publisher) if not exempted from copyright protection by the applicable law.

(Article begins on next page)

1 **DESIGN OF ACTIVE DEBRIS FLOW MITIGATION MEASURES: A COMPREHENSIVE ANALYSIS OF**  
2 **EXISTING IMPACT MODELS**

3

4 Federico Vagnon

5 Department of Earth Science, University of Turin, Via Valperga Caluso 35, 10125, Turin, Italy

6 email: [federico.vagnon@unito.it](mailto:federico.vagnon@unito.it) - Tel: +39 0116705325

7 ORCID: 0000-0003-0539-0557

8

9 **Abstract:**

10 Debris flows occur in mountainous areas characterized by steep slope and occasional severe rainstorms. The massive  
11 urbanization in these areas raised the importance of studying and mitigating these phenomena. Concerning the strategy  
12 of protection, it is fundamental to evaluate both the effect of the magnitude (that concerns the definition of the hazard),  
13 in terms of mobilized volume and travel distance, and the best technical protection structures (that concerns the  
14 mitigation measures) to reduce the existing risk to an acceptable residual one. In particular, the mitigation measure  
15 design requires the evaluation of the effects of debris flow impact forces against them. In other words, once it is  
16 established that mitigation structures are required, the impacting pressure shall be evaluated and it should be verified  
17 that it does not exceed barrier resistance.

18 In this paper the author wants to focus on the definition and the evaluation of the impacting load of debris flows on  
19 protection structures: a critical review of main existing models and equations treated in scientific literature is here  
20 presented. Although most of these equations are based on solid physical basis, they are always affected by an empirical  
21 nature due to the presence of coefficients for fitting the numerical results with laboratory and, less frequently, field data.  
22 The predicting capability of these equations, namely the capability of fitting experimental/field data, is analysed and  
23 evaluated using ten different datasets available in scientific literature. The purpose of this paper is to provide a  
24 comprehensive analysis of the existing debris flow impact models, highlighting their strong points and limits.  
25 Moreover, this paper could have a practical aspect by helping engineers in the choice of the best technical solution and  
26 the safe design of debris flow protection structures. Existing design guidelines for debris flow protection barrier have  
27 been analysed. Finally, starting from the analysis of the hydro-static model response to fit field data and introducing  
28 some practical assumptions, an empirical formula is proposed for taking into account the dynamic effects of the  
29 phenomenon.

30

31 **Keywords:** debris flow, impact models, landslide-structure interaction, predicting capability

32

33 **INTRODUCTION**

34 In the last decades, the climate changes have rapidly triggered the glacier melting, the permafrost degradation and the  
35 generation of extreme events like rapid and severe rainstorms. All these aspects have contributed to increase the  
36 possibility of occurrence of a particular type of landslide: debris flows (Zimmerman and Haerberli 1992).

37 Debris flow is a paroxysmic phenomenon due to a rapid or extremely rapid mobilization of a mixture of water, sediments  
38 and floating material into a steep channel (Iverson 1997; Hungr 2005). Their high density, greater than  $1700 \text{ kg/m}^3$   
39 (ONR-24800 2009) and high runout velocity, up to 20 m/s (Hungr et al. 2014) make them decisive in the morphological  
40 evolution of mountain areas, often extensively urbanized and therefore characterized by high hazard degree (Fioraso  
41 2000). Their worldwide diffusion and the colonization of virgin areas, joined with the world population increase, grow  
42 up the probability for debris flow to cause disasters.

43 Like avalanches, debris flows occur with little warning and exert great loads on obstacles they encounter. Like water  
44 floods, they are fluid enough to travel long distances in channels and inundate vast areas (Iverson 1997). Moreover,  
45 their unpredictability hampers collection of detailed real event data.

46 Since risks cannot be eliminated but only mitigated, many mitigation strategies have been developed in the last years.  
47 When a potential source area is identified, since stabilization is not always a practical option, the consequences of  
48 failure must be considered. The latter are the basis for the design of mitigation measures and for the management of the  
49 residual risk (Jakob et al. 2016).

50 Mitigation measures can be divided in two different types:

- 51 - Active measures, which are focused on the hazard and essentially they prevent the debris flow triggering, transport  
52 and deposition and can therefore change debris magnitude and frequency characteristics (Huebl and Steinwendtner  
53 2000; Kienholz 2003).
- 54 - Passive measures, which are focused on the potential damage and are used to change the vulnerability of debris flow  
55 either with hazard mapping (Bankoff et al. 2004; Griswold 2004) or through immediate disaster response (Kienholz  
56 2003; Badoux et al. 2009; Santi et al. 2010).

57 Although passive measures are more advisable than active ones, the latter are necessary in order to correctly manage  
58 residual risk (Jakob and Hungr 2005). A correct land-use planning and a hazard management implicate lower costs  
59 (economical and social) but usually active measures are required, especially where there was an inadequate risk  
60 management.

61 Since protection structures are designed to withstand the impact force of the moving mass, the estimation of the  
62 potential impact pressure becomes a key aspect for safely design these mitigation measures. The scientific community  
63 has widely faced the challenge of debris flow hazard assessment, but universally recognized models for the design of  
64 these structures are still missing (Vagnon et al. 2016).

65 Data availability and universal applicability are the main issues for the development of predicting impact models. The  
66 lack of data from monitoring of debris flow events forces to perform small-scale (e.g. Armanini and Scotton 1992;  
67 Huebl and Holzinger 2003; Canelli et al. 2012; Wendeler and Volkwein 2015; Ashwood and Hungr 2016; Vagnon and  
68 Segalini 2016) and full-scale flume experiments (DeNatale et al. 1999; Bugnion et al. 2012). Laboratory tests are useful  
69 but they are affected by scale effects that cannot be properly quantified and, consequently, they may not replicate or be  
70 comparable with field data (Iverson 1997; Huebl et al. 2009). Thus, their results must be interpreted with a healthy dose  
71 of scepticism (Iverson 2015) since performing analogue experiments of large scale phenomena require satisfy all the  
72 relevant similarity criteria but this is impossible for debris flows (Turnbull et al. 2015). Researchers have to choose if  
73 maintain stress similarity or lost information on particle effects. The first scenario requires increasing the effective

74 gravity and consequently, performing centrifuge experiments. The use of uniform material, as in chute experiments, is a  
75 huge simplification because produces limited pore-fluid pressure effects and excessive pore-fluid shear resistances that  
76 can lead to underestimation of solid-fluid drag and dynamic effects. Consequently, an appropriate scale analysis is  
77 always required for the study of mass movements such as debris flows.

78 In 1996, the US Geological Surveys (DeNatale et al. 1999) performed debris flow impact tests on flexible barriers in a  
79 full-scale concrete flume, highlighting that the inherent variability of a well-controlled, staged debris flow made it  
80 difficult to isolate the effect of any single parameter. Instead, Bugnion et al. (2011) in their full-scale experiments of  
81 hillslope debris flows, stated that pressures depend primarily on the flow speed, which in turn appears to depend on the  
82 grain-size distribution and water content.

83 As a consequence, even if the results of full- and small- scale tests are comparable to those observed in real-scale  
84 measurements and simulate quite well the physics of idealised debris flows, they may not describe well the rheology,  
85 the complex topography and the presence of obstacles (buildings, infrastructures etc.) along the debris flow path (Gao et  
86 al. 2017).

87 Many of these formulations yield a rough estimation of the debris flow impact pressure against structures due to their  
88 empirical nature, their validation only based on small-scale observations that could lead to high discrepancies with field  
89 observations (e.g. Hungr et al. 1984; Revellino et al. 2004; Zanchetta et al. 2004; Shen et al. 2018). Then, dimensions,  
90 types and inertial resistance of the barriers are completely neglected in most of these models (Vagnon and Segalini  
91 2016).

92 Finally, for what it concerns the model validation, it is performed on limited datasets, both in terms of number and type  
93 of observations.

94 The aim of this paper is to analyse debris flow impact models proposed in scientific literature and evaluate the  
95 discrepancies between measured and numerically predicted results using ten datasets available in scientific literature.  
96 Sixteen formulations were accurately discussed, highlighting their strong points and their shortcomings. As a result of  
97 the data analysis, a new formulation is here presented.

98 The insights carried out from this paper will be useful for engineers to design debris flow protection measures.  
99 Moreover, the presented results will help engineers in the choice of the best debris flow impact model as a function of  
100 phenomenon features and mitigation measures technical characteristics.

101 The present study is organized into six sections: the first one is introductory and presents the most common mitigation  
102 methods for debris flows. The second section provides a review of debris flow impact models. Section three  
103 summarizes current international standards in debris-flow mitigation design. In section four and five, the impact models  
104 are compared and statistically analysed for evaluating their reliability in predicting measured pressure. Finally, an  
105 empirical model is proposed and the main results of this study are summarised and discussed.

106

## 107 **DEBRIS FLOW CONTROL BY BARRIERS**

108 The use of mitigation measures depends on the adopted protection strategy and on the objectives established from the  
109 risk assessment (Huebl 2001). The choice of the best mitigation measure must be evaluated with respect to its technical,  
110 economical, ecological and political feasibility.

111 Generally, the areas susceptible to debris flow phenomena are narrow and not suitable for installing large structures.  
112 Although setting only one structure is often by no means sufficient to make debris flow harmless and, moreover an  
113 integration of both active and passive measures should be encouraged (Takahashi 2007), in the last three decades many  
114 active mitigation measures have been installed worldwide. Active debris flow mitigation measures affect the initiation

115 or the transport or the deposition of debris flows. Mitigation measures have a direct effect on the magnitude and on the  
116 frequency of the phenomenon, changing the probability of the event or manipulating the debris flow itself. They must  
117 be designed to resist the impact force and their main tasks are: i) dissipate the debris flow kinetic energy and ii) retain  
118 totally or partially the debris flow material (VanDine 1996; Mizuyama 2008; Brighenti et al. 2013; Song et al. 2017;  
119 Wendeler et al. 2018).

120 Common debris flow structural measures include close-type check dams (Fig. 1a), open-type sabo dams (Fig. 1b),  
121 concrete slit sabo dams (Fig. 1c) and flexible net barriers (Fig. 1d).

122

123 **Fig. 1** Different types of debris flow active mitigation measures: check dam (photograph by Los Angeles County Flood  
124 Control District) (a), open type Sabo structures (photograph of steel check dam in Nagano prefecture, Japan) (b),  
125 concrete slit barrier (photograph by LCW Consult web site of protection works in St. Luzia River, Madeira, Portugal)  
126 (c) and flexible net barrier (photograph by Geovertical S.R.L web site of protection works in Terranova Pollino,  
127 Basilicata Region, Italy) (d)

128

129 The design of these structures should comply with two requirements: firstly, it should take into account geographical,  
130 geological and site conditions. Secondly, at the end of design process the structural resistances shall be always greater  
131 than the effects of the forces exerted on the structure. For what it concerns the barrier resistance, it can be easily  
132 evaluated since the resistance of each single component is well known and accurately calculated. By contrast, the  
133 definition of the impacting load on the structure is an open issue (Vagnon et al. 2017a): as it will be described in the  
134 next section, there are many models for quantifying the stress distribution on the barrier, but none of them is universally  
135 recognized. Moreover, their predicting capability, that is an evaluation of the discrepancy between measured and  
136 estimated impact forces, especially using data collected from real events, is unknown. In particular, for mitigation  
137 measure designers become of utter importance to know under which dynamic features the impact models lead to an  
138 underestimation or excessive overestimation of the load conditions.

139 Finally, it is important to underline that the accuracy of dimensioning procedure is therefore highly dependent on the  
140 quality of process scenario. Inaccurate assumptions may result in inefficient design or in a partial or total failure of the  
141 structure and can lead to negative consequences for the vulnerable area. This means that poor quality input data (flow  
142 velocity, thickness, density, volume etc.) arises uncertainties in the evaluation of impacting load.

143

#### 144 **DEBRIS FLOW IMPACT MODELS**

145 For an efficient design of mitigation structures, the debris flow impact pressure exerted on barriers is of utter  
146 importance because it is the main factor that causes structural collapse (Hungry et al. 1984; Armanini 1997; Huebl et al.  
147 2009; Ferrero et al. 2015). Furthermore, there is an increasingly greater need in predicting impact load for the  
148 assessment and the management of risk.

149 Debris flow involves fundamentally independent physical and dynamical processes that couldn't be controlled by one  
150 or two parameters. The flow is heterogeneous and the mixture density evolves strongly as a function of time and space  
151 due to mixing, phase separation and particle sorting: this aspect leads to drastic change of the local material  
152 composition and it can result in huge impact pressure differences during impact (Iverson 1997). Moreover, density,  
153 velocity and flow height should be considered as field variable due to their variation through space, along the channel  
154 path, and time, during the flow process (Hungry et al. 1984; Kwan 2012). For all these reasons, the development of a  
155 reliable debris flow impact scheme results extremely complex.

156 The design of mitigation structures should require simplified models to predict impact pressure with high reliability;  
157 these models should be universally recognized and should include few parameters, related to material and flow  
158 characteristics easy to estimate.

159 Finally, the modelling of debris flow surges is difficult because the impact pressure depends on a dynamic component  
160 exerted by the heterogeneous flow, that can reach  $10 - 5 \times 10^3 \text{ kN m}^{-2}$ , and an impulsive component generated by the  
161 single impact of boulders: the latter can vary between  $10^2$  and  $10^4 \text{ kN m}^{-2}$  (Suwa and Okuda 1983; Zhang 1993).

162 Moreover, the flow composition and the impact mechanism strongly influenced the impact load and its distribution on  
163 structures (Song et al. 2017). Many studies (Choi et al. 2015; Sovilla et al. 2016; Ng et al. 2019) on this topic have  
164 highlighted that when dry granular flows impacting a rigid barrier, a pileup mechanism developed. On the contrary,  
165 viscous flows exhibited the formation of a vertical-jet mechanism upon impact. This happens when the flow inertia is  
166 larger than restoring gravitational field (Poudyal et al. 2019). In fact, in viscous flow, the effect of particle shearing in  
167 kinetic energy dissipation is less significant compared to frictional-grain stresses in dry granular flow.

168 It is obvious that debris flow modelling requires many assumptions for simplifying its real complex nature: a) the  
169 mixture has to be considered as an equivalent fluid with averaged characteristics of density, b) the simultaneous  
170 occurrence of maximum velocity and thickness values, c) the rigid behaviour of the flow at the impact (Osanaï et al.  
171 2010; Suda et al. 2010; Kwan 2012).

172 On the basis of these hypotheses, in the last decades many methods were developed and, in general, they can be  
173 classified into hydraulic and solid-collision (Huebl et al. 2009) and shock-wave propagating upstream models (Chou et  
174 al. 2012; Albaba et al. 2018).

175 Hydraulic models, derived from fluid momentum balance and Bernulli's equation, schematize the flowing mass as a  
176 homogeneous mean (characterized by an average density between fluid and solid component) and consider the load as a  
177 modified value of hydro-dynamic pressure or a multiple of the hydro-static load or a combination of both.

178 The maximum impact pressure considering hydro-static model can be evaluated using the following equation:

179

$$180 \quad p_{\text{peak}} = k \cdot \rho_m \cdot g \cdot h_f \quad (1)$$

181

182 where  $p_{\text{peak}}$  is the maximum impact load in  $\text{N m}^{-2}$ ,  $k$  is an empirical coefficient,  $\rho_m$  is the mean density of the debris  
183 impacting fluid in  $\text{kg m}^{-3}$ ,  $g$  is gravity in  $\text{m s}^{-2}$  and  $h_f$  is the flow height in m. This model is based on a triangular load  
184 distribution and the load increase factor,  $k$  (e.g. Lichtenhahn 1973; Armanini 1997). The latter can assume values  
185 ranging from 2.5 to 7.5.

186 Lichtenhahn (1973) firstly applied this equation for the evaluation of debris flow impact on concrete barrier, proposing  
187  $k$  values between 3.5 and 5.5. Later, following the same theoretical principles of the previous study and comparing  
188 results with experimental tests, Armanini (1997) evaluated  $k$  as 4.5 times the hydro-static pressure. At the same time,  
189 Scotton and Deganutti (1997), performing small scale laboratory tests and measuring impact pressure on vertical  
190 obstacle, estimated  $k$  varying between 2.5 and 7.5, depending on the viscosity of the interstitial fluid and flow hydraulic  
191 conductivity.

192 The popularity of these formulations is due to their simplicity and the few number of parameters involved: in fact they  
193 only require debris density and flow height and usually flow height is considered equal to channel depth. On the other  
194 hand, they do not take into account flow rheological properties and they are only applicable with small velocity values  
195 or rather with flatter terrain.

196 Concerning hydro-dynamic models, the impact on the structure has a constant load distribution and the general equation  
197 is:

$$198$$
$$199 \quad p_{\text{peak}} = \alpha \cdot \rho_m \cdot v_f^2 \quad (2)$$
$$200$$

201 where  $\alpha$  is the dynamic coefficient and  $v_f$  is the flow velocity in  $\text{ms}^{-1}$ .

202 The parameter  $\alpha$  include information about the flow type, the formation of vertical jet-like wave at the impact, the grain  
203 size distribution and the barrier type (Canelli et al. 2012).

204 Watanabe and Ikeya (1981) firstly applied this model for the analysis of volcanic mudflow in Japan. They found that  $\alpha$   
205 ranged between 2 and 4 as a function of the grain size distribution of the mixture.

206 The following equation is the Hungr et al.' equation (1984) and it is maybe the most famous hydro-dynamic  
207 formulation used for evaluating debris flow impact pressure against obstacles:

$$208$$
$$209 \quad p_{\text{peak}} = 1.5 \cdot \rho_m \cdot v_f^2 \cdot \sin\beta \quad (3)$$
$$210$$

211 where  $\beta$  is the least angle between the face of the barrier and the flow direction.

212 The dynamic coefficient equals to 1.5 was defined after the back-analysis of data from monitoring of real debris flow  
213 events occurred in British Columbia (Canada). This coefficient was included for considering the generation of a  
214 stagnant wedge behind protection barriers.

215 Moreover, in scientific literature exists a wide range of proposed values for the dynamic coefficient: Daido (1993)  
216 suggested values varying between 5 and 12, Zhang (1993) recommended a range between 3 and 5, Bugnion et al.  
217 (2011) measured values from 0.4 to 0.8, Canelli et al. (2012) between 1.5 and 5.

218 The values listed above prove that the range of variation of dynamic coefficient (between 0.4 and 12) deeply conditions  
219 the evaluation of peak pressure: consequently, from an engineering point of view, the design of protection barriers is  
220 strongly influenced by the choice of one formulation respect to another, arising uncertainties in the reliable evaluation  
221 of the probability of failure of the mitigation measure.

222 Huebl and Holzinger (2003) developed a modified hydro-dynamic formula introducing Froude number ( $F_r$ ) to  
223 normalised impact force and achieved a scale-independent relationship:

$$224$$
$$225 \quad p_{\text{peak}} = 5 \cdot \rho_m \cdot v_f^{0.8} \cdot (g \cdot h_f)^{0.6} \quad (4)$$
$$226$$

227 Using small-scale flume experiments and 155 sets of data coming from other authors, Cui et al. (2015) estimated the  
228 peak impact pressure as:

$$229$$
$$230 \quad p_{\text{peak}} = 5.3 \cdot F_r^{-1.5} \cdot \rho_m \cdot v_f^2 \quad (5)$$
$$231$$

232 Combining Equation 1 and 2, many Authors hypothesized new relationships to estimate maximum impact pressure  
233 against barrier. The general relation is:

$$234$$
$$235 \quad p_{\text{peak}} = \rho_m \cdot g \cdot h_f + \rho_m \cdot v_f^2 \quad (6)$$
$$236$$

237 Cross (1967) firstly modified the equation for perfect fluid used for evaluating tsunami impact forces introducing static  
 238 coefficient,  $k$ , and dynamic coefficient,  $\alpha$ , respectively equal to 0.5 and 3 as follow:

239

$$240 \quad p_{peak} = k \cdot \rho_m \cdot g \cdot h_f + \alpha \cdot \rho_m \cdot v_f^2 \quad (7)$$

241

242 Later, Arattano and Franzi (2003), analysing measured data in Moscardo Torrent (Italy), validated Equation 6.

243 Other studies were carried out hypothesizing the total reflection of a flow against a vertical wall and, imposing the  
 244 dynamic equilibrium (Lamberti and Zanuttigh 2004). The relation is:

245

$$246 \quad p_{peak} = C_c \cdot \frac{(1+\sqrt{2}F_r)^2}{2} \cdot \rho_m \cdot g \cdot h_f \quad (8)$$

247

248 where  $C_c$  is an empirical coefficient calibrated considering the vertical acceleration caused by the presence of fine  
 249 particles and boulder equal to 1.5.

250 Another equation to evaluate the dynamic impact of a debris flow against a vertical wall is presented by Armanini et al.  
 251 (2011):

252

$$253 \quad p_{peak} = \left(1 + \frac{1}{2} \cdot F_r^2\right) \cdot \left(1 + \frac{\alpha \cdot F_r^2}{1 + \frac{1}{2} F_r^2}\right) \cdot \rho_m \cdot g \cdot h_f \quad (9)$$

254

255 where  $\alpha$  is a coefficient equal to 1.

256 Recently, Vagnon and Segalini (2016), performing several small scale flume tests, proposed a new model that takes into  
 257 account either flow characteristics, material properties and barrier dimensions. The numerical expression is given as:

258

$$259 \quad p_{peak} = \left(\frac{1}{2} K_a (n^2 - 1) \cos\theta + \alpha F r^2 \cos\beta - \tan\varphi' \frac{n-1}{\sin\theta} \cos\beta \cos\theta\right) \rho_m g h_f \quad (10)$$

260

261 where  $K_a$  is active lateral earth pressure coefficient derived from Rankine theory,  $\theta$  is slope angle in deg,  $\beta$  is the angle  
 262 between the barrier and the normal at channel bottom, measured in deg,  $\varphi$  is the debris friction angle in deg and  $n$  is the  
 263 filling ratio, that is the ratio between the barrier height and the flow height. In this relation, dynamic coefficient,  $\alpha$ , can  
 264 vary between 0.5 and 1.2.

265 Solid-collision models are based on the Hertz contact theory as the following:

266

$$267 \quad F_B = K_c n a^{1.5} \quad (11)$$

268

269 where  $K_c$  is the load reduction factor that depends on barrier stiffness (Hung et al. 1984; Kwan 2012; Ng et al. 2016),  $n$   
 270 takes into account the radius of impacting boulder, its Poisson's ratio and the Young's modulus of the boulder itself and  
 271 the barrier. The parameter  $a$ , depends on boulder mass and impact velocity. In scientific literature, many solid-collision  
 272 models have been presented (Kwan 2012; Faug 2015; Ng et al. 2016; Song et al. 2017): their use is related to the ratio  
 273 between boulder dimension and debris flow thickness. Ng et al (2016) highlighted that if this ratio is lower than 0.6,  
 274 solid-collision contribution can be neglected and the impact of debris flow can be calculated using Equation 2 with  $\alpha$   
 275 equals to 2.5.

276 For what it concerns shock-wave models, the impacting force is considered as a combination of inertial and depth-  
277 dependent forces associated with features of the incoming flow (Albaba et al. 2018). Although the shock-wave solution  
278 is obtained from the jump conditions of the mass and momentum balances, its predictions are in good agreement with  
279 experimental results (Chou et al. 2012). The main limitation of these methods is the high sensitivity of peak force to  
280 sampling length (that defines the sample dimension for averaging flow motion characteristics): in particular, Albaba et  
281 al. (2018) highlighted that only for slope angle greater than  $42.5^\circ$  and sampling length greater than 35 times the average  
282 particle diameter, the peak force is well predicted.

283 One further remark has to be made concerning the use of all the presented methods in numerical modelling: many  
284 numerical codes (Hutter et al. 1994; Brighenti et al. 2013; Albaba et al. 2015; Ashwood and Hungr 2016; Leonardi et al.  
285 2016; Vagnon et al. 2017b; Wendeler et al. 2018) have been developed on the basis of hydro-static and hydro-dynamic  
286 simplified approach.

287 In this paper only hydraulic models has been treated and discussed, since not all the necessary parameters were  
288 available for evaluating the contribution of solid-collision and shock-wave models.

289 Table 1 summarizes general equations of all the previous models, highlighting the range of variation for static ( $k$ ) and  
290 dynamic ( $\alpha$ ) coefficient. Moreover, Table 1 includes information about the texting procedure and how  $\alpha$  and  $k$   
291 coefficients were evaluated (cfr. columns three and four of Table 1). These coefficients depend on the type of mitigation  
292 measure considered and the characteristics of flow, in terms of grain size and viscosity. Mainly, they were calibrated  
293 performing small-scale tests on rigid (e.g. Armanini 1997; Scotton and Deganutti 1997; Kwan 2012) or flexible barriers  
294 (e.g. Canelli et al. 2015; Ashwood and Hungr 2016; Wendeler et al. 2018) and more rarely, they were evaluated as a  
295 result of full-scale test or real debris flows (Arattano and Franzi 2003; Bugnion et al. 2011).

296

297 **Table 1** – Summary of analysed hydraulic model for evaluating peak debris impacting pressure on barriers.

298

## 299 **INTERNATIONAL GUIDANCES FOR MITIGATION DESIGN: AN OVERVIEW**

300 At present, there are few existing international technical guidelines about debris flow mitigation measures, one of which  
301 is undoubtedly the ONR series (ONR 24800 to ONR 24803) developed by the Austrian “Wildbach und  
302 Lawinenverbauung” office (WLV). The debris flow load models and the design, construction and life cycle assessment  
303 of protection works are arranged in these standards (Suda et al. 2010). In particular, ONR 24801 defines two models for  
304 calculating debris flow impact pressure: the first one, named as simple model, is based on Equation 1, assuming that  $h_f$   
305 is equal to the barrier height and  $k$  ranges normally between 3 to 6. The second one, named as complex model,  
306 corresponds to Equation 4. In both cases, the standard specifies that flow parameters must be given by an expert for  
307 torrential control. Moreover, twelve stress combinations are defined depending on the functional type of mitigation  
308 structure in order to take into account uncertainties and provide adequate design of mitigation measure. At European  
309 level, ONR series are the only standards concerning debris flow mitigation structure design: recently, the European  
310 Organisation for Technical Assessment published the new European Assessment Document (EAD 340020-00-0106  
311 2016) concerning the flexible kits for retaining debris flows and shallow landslides/open hill debris flows. This  
312 regulation defines the main components and the methods to assess the performance of the kit. These guidelines concern  
313 only the certification of barrier performances but no information on load distribution are given.

314 Other existing standards are the Japanese NILIM (National Institute for Land and Infrastructure Management) 904 and  
315 905 (Osanaï et al. 2010) that define the design characteristics of Sabo barriers. Compare to Austrian ONR series, these  
316 guidances are less specific (Moase 2017) since they suggest considering different combination of external forces (static

317 water pressure, sediment pressure and fluid forces of debris flow) without providing any formulations for their  
318 calculation.

319 One of the most comprehensive standard is that developed by Geotechnical Engineering Office (GEO) of Hong Kong.  
320 In particular, the GEO report 270 (Kwan 2012) presents guidelines on the design of debris-resisting barrier. For what it  
321 concerns impact model, the design guidance recommends that the design loading on barrier is based on multi-surge  
322 scenario and the total load is considered as the sum of dynamic impact and boulder impact (if the existence of boulders  
323 or large hard inclusions in the flow cannot be precluded). Boulder impact should be calculated using the simplified form  
324 of Equation 11 as following:

$$325 \\ 326 F = K_c 4000 v^{1.2} r^2 \quad (12)$$

327  
328 where  $K_c$  is equal to 0.1,  $v$  is the boulder impact velocity normal to the barrier and  $r$  is the radius of boulder. Dynamic  
329 load should be calculated using Equation 2 with  $\alpha$  equals to 2.5.

330 Analysing the previous standards, it is clear that there is not a universally recognized impact model: each guideline is  
331 based on local experience of use of debris resisting barriers.

332

### 333 **EVALUATION OF THE PREDICTING CAPABILITY OF DEBRIS FLOW IMPACT MODELS**

334 As stated above, the design of mitigation measures requires defining the load exerted by the flow on structures. The  
335 equations listed in Table 1 show that universally recognize model does not exist and thus it becomes fundamental for  
336 designers to know the capability of these models to fit experimental and field measurements. The choice of a model in  
337 relation to another mainly depends on: a) how accurately is the calculated pressure compared to the measured one; b)  
338 the limitations (if any) in the applicability of the model.

339 The predicting capability of the previous models was evaluated by comparing the predicted results with data coming  
340 from ten different datasets available in scientific literature. As listed in Table 2, their choice was made on the basis of  
341 availability of both dynamic information (thickness, velocity and density) and impact features (impact load) and for  
342 ensuring that the datasets covered different testing scenarios (soil type, water content, channel slope, magnitude) and  
343 different scale approaches. The datasets included values of flow velocity, thickness and impacting peak pressure  
344 collected from small scale tests performed in specifically created flumes (Scheidl et al. 2013; Cui et al. 2015; Ashwood  
345 and Hungr 2016; Vagnon and Segalini 2016), from full-scale debris flow (DeNatale et al. 1999; Bugnion et al. 2011)  
346 and from monitoring of recurrent debris flow in the Jiangjia Ravine basin in China (Hu et al. 2011; Hong et al. 2015)  
347 and Illgraben debris flow monitoring site in Switzerland (McArdell 2016; Wendeler et al. 2007).

348 Moreover, The choice of analysing both small-scale tests and field data was made to understand if the approach here  
349 presented could produce reliable results and to dispel any doubts on the result interpretation. The author is conscious  
350 that miniaturized tests are affected by scale effects and investigated materials are usually not satisfyingly representative  
351 of material involved in debris flow phenomena, but if a trend is recognized in both datasets, the analysis can be  
352 considered as a sign of a reliable approach.

353 In this paper, the data of peak impact pressure were normalized by those of hydro-static pressure as follows:

354

$$355 \check{p} = \frac{p_{peak_{measured}}}{\rho \cdot g \cdot h_f} \quad (13)$$

356

357 These values were plotted as a function of the Froude number,  $Fr$ , of the flow in order to achieve scale-invariant  
358 description. Froude number is defined as the square root of the ratio between kinetic and gravity force of the flow and it  
359 is useful for demarcating quasi static rate-independent from speed-squared force contributions (Faug 2015). An  
360 important remark has to be done for the evaluation of  $Fr$  values: a recent study published by Ng et al. (2019) highlighted  
361 that the choice of frontal velocity and maximum flow depth within the frontmost region of the flow is crucial for  
362 properly characterising the impact mechanism. In particular, an estimation of non-frontal  $Fr$  values may lead to an  
363 underestimation of impact pressure by a factor of two.

364 In general, laboratory and field data accordingly show the same range of variation of the normalized peak pressure; for  
365 what it concerns the Froude number, the range of variation related to laboratory tests is wider than the field one. As  
366 stated above, this discrepancy can be attributed to scale effects. However, the two dataset globally have the same trend  
367 for  $\tilde{p}$  as function of  $Fr$ .

368 The normalized pressures,  $\tilde{p}$ , were compared to all the listed above predicting models, considering for each one the  
369 upper and the lower limit of the range of variability of empirical coefficients  $k$  and  $\alpha$ . For the sake of simplicity and  
370 readability of figures, the models were pooled into three groups (hydro-static, hydro-dynamic and mixed models) and  
371 plotted separately for better highlighting limitations and strong points for each model.

372 In Fig. 2, the predicting capability of hydro-static models is evaluated: in general, these formulations underestimate the  
373 normalized peak pressure measured both in small- and full-scale tests (Fig.s 2a and 2b) and field data (Fig. 2c),  
374 regardless of the value of empirical coefficient  $k$ .

375 In general, from an engineering point of view, the fact that hydro-static models underestimate the debris flow impact  
376 pressure (with the exception of Scotton and Deganutti (1997) model with  $k = 7.5$  for  $Fr$  lower than 3) points out an  
377 inadequacy for the design of protection structures.

378

379 **Fig. 2** Comparison between normalized debris flow impact force and hydro-static predicting models as function of  
380 Froude number considering small- (a) and full-scale experiments (b) and field data (c).

381

382 For a deeper analysis, the ratio between the measured peak pressure and the estimated one was calculated and reported  
383 in Fig. 3 as function of Froude number for both small- (a, d) and full-scale (b, e) and field datasets (c, f). The upper  
384 (7.5) and the lower (2.5) limits of the  $k$  range of variation were chosen in order to define the suitability for predicting  
385 impact pressure of the hydro-static models.

386 The peak pressure ratio gives information about the discrepancy between predicted results using hydro-static methods  
387 and measured ones: if this ratio is lower than 1, the predicting value overestimates the measured one, vice-versa the  
388 peak pressure is underestimated. If this ratio is 1, there is a perfect correspondence (green continuous line in Fig. 3)  
389 between measured values and predicted one. From an engineering point of view, for providing safe results, predicting  
390 models should exhibit a ratio lower than unity, and in particular varying between 0.5 and 1, so that the impacting  
391 pressure is reasonably overestimated. This aspect will be better explained in the next section.

392 Analysing Fig. 3, hydro-static formula with  $k = 2.5$  (that corresponds to the lower limit of Scotton and Deganutti (1997)  
393 equation) always underestimates the measured peak pressure (Fig.s 3a to 3c). On the contrary, Scotton and Deganutti  
394 (1997) equation considering  $k = 7.5$  simulates well about the 55% of the field data (Fig. 3f). These two equations define  
395 the variability domain of the existing hydro-static formulations.

396 Analysing Fig. 2 and Fig. 3, there is an evident non-linear relation between estimated pressure and Froude number: the  
397 higher is  $Fr$  a, the higher is the distance between measured and estimated pressure value. Moreover, considering

398 Scotton and Deganutti (1997) formulation (with  $k = 7.5$ ), it seems that the prediction capability of this model is high for  
399  $Fr < 3$ ; in this case the percentage of peak pressure ratio lower than 1 increases till 70%.

400 It becomes obvious that hydro-static models are suitable only for low Froude numbers (generally lower than 3, Huebl  
401 and Holzinger 2003; Cui et al. 2015), namely when the flow is characterized by low velocity and dynamic components  
402 are negligible (Huebl and Holzinger 2003) (cfr. Fig. 3).

403 In this study, starting from this observation, an attempt to take into account dynamic effects in hydro-static models will  
404 be presented and discussed.

405

406 **Fig. 3** Relationship between measured peak pressure and calculated hydro-static peak pressure with  $k$  respectively equal  
407 to 2.5 (a to c) and 7.5 (d to f) as a function of the Froude number considering both small- (a, d) and full- scale (b, e) and  
408 field dataset (c, f). The green continuous line represents the perfect correspondence between measured values and  
409 estimated ones.

410

411 Concerning hydro-dynamic models, they have a good capability in predicting the peak impact pressure (Fig. 4) except  
412 for models with dynamic coefficient,  $\alpha$ , lower than 1 (Bugnion et al. (2011), cfr. Fig.s 5a to 5c). The two key points are:  
413 a) verify if the predicting capability is influenced by flow regime; b) considering maximum dynamic coefficient value  
414 ( $\alpha = 12$  from Daido (1993)) the peak values are excessively overestimated. The latter point has a great impact on the  
415 design of mitigation measures, in particular on their construction costs (cfr. next section).

416 In Fig. 4a, for very low Froude values ( $Fr < 2$ ), it seems that hydro-dynamic models are affected by of the influence of  
417 flow regime, characterized by low velocity and high impact thickness. In this case, only Daido (1993) equation reaches  
418 to satisfactorily predict peak pressure.

419

420 **Fig. 4** Comparison between normalized debris flow impact force and hydro-dynamic predicting models as function of  
421 Froude number considering small- (a) and full-scale tests (b) as well as field data (c).

422

423 Focusing on Hungr et al. (1984) equation (continuous blue line in Fig. 4), which is certainly the most famous, in the  
424 86% of cases it overestimates the measured peak pressure. This formulation has a high predicting capability for high  
425 Froude values, meanwhile for Froude equal or lower 2 it underestimates measured pressure (Fig.s 4a and 4c). In Fig. 5,  
426 this aspect is better clarified: observing the pressure ratio, it decreases when Froude number increases following an  
427 inverse power law. Except for Bugnion et al (2011) equation (Fig.s 5a to 5c) for which the pressure ratio is almost never  
428 lower than unity, in the other formulations this relationship is verified for  $Fr > 2$ . Daido (1993) formulation with  $\alpha = 12$   
429 (Fig.s 5d to 5f) deserves a debate of its own: in fact it excessively overestimates the pressure values (except for  $Fr < 2$ ,  
430 confirming the observation made above), reducing pressure ratio close to 0. This latter point will be better argued in  
431 next section.

432

433 **Fig. 5** Relationship between measured peak pressure and calculated hydro-dynamic peak pressure with  $\alpha$  respectively  
434 equal to 0.4 (a to c) and 12 (c to d) as a function of the Froude number considering both small- (a, d) and full-scale (b,  
435 e) and field dataset (c, f)

436

437 Summarizing, the analysis performed on small- and full-scale and field data has highlighted that pure hydro-static and  
438 pure hydro-dynamic models are not totally adequate to predict debris flow impact pressure on structures. In Froude

439 region lower than 3, where velocity are low and impacting thickness are high (cfr. Fig. 6) hydro-static formulations  
440 perform well; on the contrary, hydro-dynamic models underestimate pressure values since kinetic effect are not  
441 dominant (Huebl and Holzinger 2003, Cui et al. 2015; Faug 2015).

442

443 **Fig. 6** Relationship between velocity (blue squares) and thickness (red diamonds) as function of Froude number for  
444 small-scale tests (a) and full-scale and field data (b). A negative correlation exists between velocity and thickness: when  
445 Froude number increases, velocity increases and consequently flow height decreases and vice-versa.

446

447

448 In the light of previous observations, mixed models are more suitable for predicting impact loads as clearly showed in  
449 Fig. 7 in which all data (both from small- and full-scale tests and field measurements) fall into the region defined by  
450 these formulations.

451

452 **Fig. 7** Comparison between normalized debris flow impact force and mixed predicting models as function of Froude  
453 number considering small- (a) and full-scale test (b) as well as field data (c).

454

455 For evaluating the performance of each formulation, the peak pressure ratio was evaluated, as shown in Fig. 8. For  
456 readability of the figure, only field data were plotted. However, mixed models showed the same behaviour regardless  
457 the choice of dataset. Generally, despite their prediction capability is more suitable than hydro-static and hydro-  
458 dynamic formulations, not all mixed models can be universally usable in practise. For instance, Huebl and Holzinger  
459 (2003) and Cui et al. (2015) equations perform well for Froude values lower than 3 (Figs 8a and 8b). Arattano and  
460 Franzi (2003) formulation provides a good correspondence between field data and predicted ones: on the contrary,  
461 Cross (1967) equation excessively overestimates pressure peak values (providing a peak pressure ratio close to 0, cfr.  
462 Fig. 8c). Armanini et al. (2011) equation shows a neglecting dependence with Froude number, which causes,  
463 particularly for low values ( $Fr < 2$ ), an underestimation of the peak pressure (Fig. 8e). This dependence is not evident in  
464 the other models (Fig. 8c and 8f).

465

466 **Fig. 8** Relationship between measured peak pressure and calculated peak pressure for different mixed models as a  
467 function of the Froude number considering field dataset (a to f).

468

## 469 **A COMPREHENSIVE STATISTICAL ANALYSIS OF PREDICTING IMPACT MODEL**

470 In this section, the predicting capability of debris flow impact models has been statistically analysed.

471 In Table 3, the results of the comparison between all the described models and small- and full-scale/field datasets are  
472 presented. The percentage is referred to the number of predicted values greater than measured ones. This condition  
473 occurs when the model overestimates the impacting peak pressure. If the percentage is high, the model has a good  
474 capability of overestimating measured peak pressure; on the contrary, if the percentage is low, the model is not suitable  
475 for predicting impact pressure. However, the percentage of overestimated peak pressure values is not sufficient for  
476 evaluating the reliability of a predicting model. From an engineering point of view the excessive overestimation shall be  
477 avoided as much as underestimation since it is related to mitigation measure construction costs. Thus, for each models  
478 was calculated the percentage of data that fall into four classes of peak pressure ratio, defined as follow:

- 479 - From 0 to 0.5 (orange class): it represents an excessive overestimation and consequently higher construction  
480 costs. If the predicting model shows a high percentage of data in this class, it should be discarded.
- 481 - From 0.5 to 0.7 (yellow class): if the predicting model shows a high percentage of data in this class, a careful  
482 analysis of cost benefit should be conducted when considering the suitability of the model.
- 483 - From 0.7 to 1 (green class): if the predicting model shows a high percentage of data in this class, it is  
484 extremely accurate in estimating impact pressure.
- 485 - From 1 to 1.3 (yellow class): taking into account the uncertainties related to parameter measurement, a careful  
486 analysis should be performed for choosing or discarding the model.
- 487 - Greater than 1.3 (red class): if the predicting model shows a high percentage of data in this class, it is not  
488 suitable for estimating debris flow impact pressure.

489 This classification gave indications about the level of overestimation/underestimation, which is important especially for  
490 defining the degree of safety of the mitigation measure and, indirectly, its construction costs.

491 Figures 9 to 11 add more information to Table 3 about predicting capability of analysed impact models: in general, all  
492 the hydro-static models (Fig. 9) are not suitable to describe debris flow impact behaviour since they have a high  
493 percentage (greater than 30%) of values that fall into red class, regardless the  $k$ -coefficient value. Hydro-dynamic  
494 formulations have a high propensity to excessively overestimate impact pressure when  $\alpha > 2$  (Fig.s 10d to 10h). Vice-  
495 versa, when dynamic coefficient is lower than unit (Fig.s 10a and 10b), these models are not suitable for predicting  
496 impact load. Hungr et al. (1984) and Canelli et al. (2012) models with  $\alpha = 1.5$  (Fig. 10c) seem to be a good compromise  
497 between overestimation and prediction capability. Except for Croos (1967) equation (Fig. 11a) that exhibits an  
498 excessive overestimation, mixed models prove their adequacy as predicting methods since they show high percentage of  
499 values that fall into green class. In particular, Arattano and Franzini (2003), Armanini et al. (2011) and Vagnon and  
500 Segalini (2016) models (Fig.s 11b, 11c and 11g) result the most suitable for predicting real debris flow impact on  
501 structures due to the high percentage of data that fall into green class (more than 40%).

502

503 **Fig. 9** Predicting capability analysis of hydro-static models using field dataset.

504

505 **Fig. 10** Predicting capability analysis of hydro-dynamic models using field dataset.

506

507 **Fig. 11** Predicting capability analysis of mixed models using field dataset.

508

## 509 TOWARDS A GENERALISED IMPACT MODEL

510 As highlighted in previous Sections, hydro-static formulations can be used, with a reliable degree of safety, to predict  
511 impact pressure for flows with  $Fr < 3$ . Moreover, analysing Table 3 and Fig. 9, it is evident how the predicting  
512 capability of these methods is very low: considering the highest  $k$  value, less than 55% of the peak pressure values are  
513 overestimated. This aspect cannot be neglected by mitigation measure designers and consequently, it makes these  
514 formulations not completely suitable for the estimation of impact forces on structures.

515 In the light of these aspects, is it possible to revise hydro-static model, improving its capability to overestimate field  
516 data?

517 Fig. 12 shows that a power law governs the trend between peak pressure ratio and Froude number. In particular the  
518 relation is:

519

520 
$$\frac{p_{peak,measured}}{\rho \cdot g \cdot h_f} = a \cdot Fr^b \tag{14}$$

521

522 where  $a$  and  $b$  are respectively equal to 1.38 and 1.64.

523

524 **Fig. 12** Relationship between field measurements of the peak pressure and calculated peak pressure using hydro-static  
525 formulation with  $k = 1$  as a function of the Froude number of the flow

526

527 Starting from Equation 14 and taking into account that estimated values should overestimate measured ones, the  
528 following modified hydro-static equation is proposed:

529

530 
$$p_{peak} = 1.5 \cdot a \cdot Fr^b \cdot \rho \cdot g \cdot h_f = k^* \cdot \rho \cdot g \cdot h_f \tag{15}$$

531

532 where  $a$  and  $b$  are respectively equal to 1.38 and 1.64 as derived from data interpolation (Fig. 12) and 1.5 is an  
533 increasing coefficient for overestimating the impact pressure. The choice of 1.5 is done in order to obtain an average  
534 peak pressure ratio of 0.8 (red line in Fig. 13) so that the estimated pressure is reasonably overestimated.

535 It has been observed that in 86% of cases this formulation overestimates field data; this percentage is comparable with  
536 that obtained using hydro-dynamic and mixed models. The statistical analysis of predicting capability is comparable  
537 with that of mixed model, with high percentage of values falling into yellow and green classes (Fig. 13b). Moreover,  
538 analysing Fig. 13a, the Froude dependence exhibited by classic hydro-static models (cfr. Fig. 2 and Fig. 3) is not present  
539 in this modified formulation. On average, the peak pressure ratio (as function of  $Fr$ ) has a horizontal trend. Only in  
540 correspondence of  $Fr = 2$ , few estimated values underestimate measured ones; however this aspect also occurs in Fig. 2  
541 and Fig. 3 for other hydro-static models.

542

543 **Fig. 13** Relationship between peak pressure ratio for the modified hydro-static model as a function of the Froude  
544 number (a) and statistical evaluation of the predicting capability of the proposed model (b).

545

546 This new formulation, although it follows the same theoretical concepts of hydro-static models, has an empirical nature  
547 since its empirical coefficient results from the analysis of field data. Fig. 14 shows the comparison between the  
548 proposed equation and the impact models that, on the basis of the previous statistical analysis, have exhibited the best  
549 predicting capability. Moreover, Lamberti and Zanuttigh (2004) and Armanini et al. (2011) models have some  
550 similarities with the proposed. In fact, the three formulations have analogous trends of  $\tilde{p}$  as function of  $Fr$ ; in general,  
551 mixed hydro-static models overestimate field data, particularly with high  $Fr$ , compared to the proposed one. Moreover,  
552 the new formulation introduces (on the basis on the used field dataset) the concept of reasonable overestimation (the  
553 increasing value of 1.5 of Equation 15 has been chosen for obtaining peak pressure ratio equals to 0.8) that it is not  
554 taken into account by other formulations. Obviously, the empirical coefficient  $k^*$  should be reviewed increasing field  
555 data in order to reach more robust statistical analyses.

556

557 **Fig. 14** Comparison between the proposed model (black line) and others hydro-dynamic (Hungr et al. 1984 and Canelli  
558 et al. 2012) and mixed (Arattano and Franzi 2003, Huebl and Holzinger 2003, Lamberti and Zanuttigh 2004, Armanini  
559 et al. 2011, Cui et al. 2015 and Vagnon and Segalini 2016) models.

560

## 561 **DISCUSSION AND CONCLUSIONS**

562 In this paper, sixteen debris flow impact models have been described and their predicting capability, or better their  
563 capability to fit experimental and field data, has been evaluated using three different dataset: one coming from small-  
564 scale flume tests, one from full-scale experiments and one from real data collected at Jiangjia Ravine (China) and  
565 Illgraben (Switzerland) basins. At first sight, the small-scale dataset showed dimensionless pressure values shifted to  
566 higher Froude numbers compared to those obtained from on-site dataset. This difference is a consequence of the scale  
567 effects that affect the small-scale tests and probably due to the influence of the triggering mechanism.

568 This study is a first attempt to compare the most famous debris flow impact models, analysing their strong points and  
569 limitations and evaluating their capability of fitting experimental and field data for helping designers in the choice of  
570 the best models to design mitigation measures (Kwan 2012).

571 For the sake of simplicity and for a direct comparison between the described methods, the models have been classified  
572 into three groups: hydro-static, hydro-dynamic and mixed models. For each model, key points and limitations have been  
573 highlighted and the main findings can be summarized as follow:

- 574 1. Hydro-static models require few input parameters (flow density and thickness) for evaluating impact pressure on  
575 structures. This aspect is particularly important for what it concerns the level of uncertainties coming from the  
576 whole debris flow scenario: since these parameters can be easily evaluated analysing past events, the result  
577 variability depends mainly by the dimensionless coefficient  $k$ . By contrast, the performed analyses have shown  
578 that the predicting capability reached an acceptable level of safety for Froude number lower than 3. Moreover, the  
579 predicting capability decreases of about the square of the Froude number, confirming that when the velocity of the  
580 flow increases (and consequently the flow thickness decreases) these models are not able to predict impact load.  
581 The performed statistical analysis also confirmed the limited suitability of these models.
- 582 2. Hydro-dynamic models provide impact pressure considering the flow density and the square velocity of the flow.  
583 The latter parameter is particularly difficult to measure during debris flow event and for this reason the related  
584 uncertainties can result high. As highlighted above, except for those models with  $\alpha$  lower than 1 (Bugnion et al.,  
585 2011), hydro-dynamic formulations have a good capability to predict and overestimate impact pressure especially  
586 for high Froude numbers (predicting capability is low when  $Fr$  is lower than 2). However, the main limitation is  
587 the excessive overestimation in predicting impact load that may results in a large increment of costs for structure  
588 construction. A dynamic coefficient equal to 2 is suggested, as a good compromise between predicting capability  
589 and excess of overestimation.
- 590 3. Mixed models seem to be best methods for predicting debris flow impact pressure on barriers, since they include  
591 both information about the static and the dynamic component of the flow. The increase in the numbers of  
592 parameters increases the uncertainties and, consequently, the degree of reliability of these methods decreases.

593 The main hypothesis behind the described methods is that the entire load is totally transferred to the structure, without  
594 any dissipation during the impact. In terms of barrier design, this hypothesis should lead to over-conservative design  
595 since stiffness and drainage capability are not taken into account. Analysing field results, the overestimation induced by  
596 this hypothesis is not always verified probably due to the hit of single boulders on the barrier, condition that required  
597 the introduction of specific equations (Kwan 2012; Faug 2015; Ng et al. 2016; Song et al. 2017) or the increase of the  
598 dimensionless coefficient ( $k$  and  $\alpha$ ).

599 Finally, the model proposed in this paper exhibits a good capability to predict impact load. It is able to take into account  
600 both the static and the dynamic behaviour of the flow without being affected by of the influence of flow regime. Further  
601 monitoring field data will be helpful eventually to review the statistics at the basis of this new formulation and to

602 improve its predicting capability. Moreover, additional monitoring debris flow systems would be very welcome to  
603 improve the knowledge about these disastrous phenomena and help to design mitigation measures with increasing level  
604 of safety and reliability.  
605 It is expected that the results proposed in this paper will be useful for designer, helping them for the best choice of  
606 debris flow impact models on barriers.

607 **References**

- 608 Albaba A, Lambert S, Nicot F, Chareyre B (2015) Relation between microstructure and loading applied by a granular  
609 flow to a rigid wall using DEM modeling. *Granular matter* 17(5):603-616.  
610
- 611 Albaba A, Lambert S, Faug T (2018) Dry granular avalanche impact force on a rigid wall: Analytic shock solution  
612 versus discrete element simulations. *Physical Review E* 97:052903-1–12.  
613
- 614 Arattano M, Franzi L (2003) On the evaluation of debris flows dynamics by means of mathematical models. *Nat*  
615 *Hazards Earth Syst Sci* 3:539–544. doi:10.5194/nhess-3-539-2003.  
616
- 617 Armanini A, Scotton P (1992) Experimental analysis on the dynamic impact of a debris flow on structures. In  
618 *Proceedings of the International Symposium Interpraevent*. Bern, Switzerland 107–116.  
619
- 620 Armanini A (1997) On the dynamic impact of debris flows. Recent developments on debris flows. In: Armanini A. and  
621 Michiue M. (eds) *Lecture notes in Earth Sciences* 208–224. Springer, Berlin.  
622
- 623 Armanini A, Larcher M, Odorizzi M (2011) Dynamic impact of a debris flow front against a vertical wall. *Ital J Eng*  
624 *Geol Environ* 1041–1049.  
625
- 626 Ashwood W, Hungr O (2016) Estimating the total resisting force in a flexible barrier impacted by a granular avalanche  
627 using physical and numerical modeling. *Can Geotech J* 53(10):1700-1717.  
628
- 629 Badoux A, Graf C, Rhyner J, Kuntner R, McArdell BW (2009) A debris-flow alarm system for the Alpine Illgraben  
630 catchment: design and performance. *Nat Hazards* 49:517–539.  
631
- 632 Bankoff G, Frerks G, Hilhorst D (eds) (2004) *Mapping vulnerability: disasters, development and people*. Earthscan,  
633 London  
634
- 635 Brighenti R, Segalini A, Ferrero AM (2013) Debris flow hazard mitigation: a simplified analytical model for the design  
636 of flexible barriers. *Comp Geotech* 54:1-15.  
637
- 638 Bugnion L, McArdell BW, Bartelt P, Wendeler C (2011) Measurements of hillslope debris flow impact pressure on  
639 obstacles. *Landslides* 9:179–187.  
640
- 641 Canelli L, Ferrero AM, Migliazza M, Segalini A (2012) Debris flow risk mitigation by the means of rigid and flexible  
642 barriers – experimental tests and impact analysis. *Nat Hazards Earth Syst Sci* 12:1693–1699. doi:10.5194/nhess-12-  
643 1693-2012.  
644
- 645 Choi CE, Au-Yeung SCH, Ng CWW (2015) Flume investigation of landslide granular debris and water run-up  
646 mechanisms. *Géotechnique Letters* 5(1):28–32.  
647

648 Chou SH, Lu LS, Hsiau SS (2012) DEM simulation of oblique shocks in gravity-driven granular flows with wedge  
649 obstacles. *Granular Matter* 14(6):719-732.  
650  
651 Cross RH (1967) Tsunami Surge Forces. *Journal of the Waterways and Harbors Division, ASCE* 93(4):201-231.  
652  
653 Cui P, Zheng C, Lei Y (2015) Experimental analysis on the impact force of viscous debris flow. *Earth Surface Process  
654 and Landforms* 40:1644–1655.  
655  
656 Daido A (1993) Impact force of mud debris flows on structures, Technical Session B. In *Proceedings of the XXV IAHR  
657 Congress*. Tokio, Japan 211–213.  
658  
659 DeNatale JS, Iverson RM, Major JJ, LaHusen RG, Fiegel GL, Duffy JD (1999) Experimental Testing of Flexible  
660 Barriers for Containment of Debris Flows. *USGS Open File Report* 38:99-205.  
661  
662 EAD 340020-00-0106 (2016) Flexible kits for retaining debris flows and shallow landslides/open hill debris flows.  
663  
664 Faug T (2015) Macroscopic force experienced by extended objects in granular flows over a very broad Froude-number  
665 range. *Eur Phys J E* 38(34):1-10.  
666  
667 Ferrero AM, Segalini A, Umili G (2015) Experimental tests for the application of an analytical model for flexible debris  
668 flow barrier design. *Engineering Geology* 185: 33-42.  
669  
670 Fioraso G (2000) Indagini geologico-morfologiche su aste torrentizie della valtellina e della Valle di Susa  
671 ricorrentemente soggette a colate detritiche torrentizie (debris flow). *Quaderni di studi e documentazione* 23,  
672 *Supplemento GEAM* 1:3-59 (in Italian)  
673  
674 Gao L, Zhang LM, Chen HX (2017) Two-dimensional simulation of debris flow impact pressures on buildings.  
675 *Engineering Geology* 226: 236-244.  
676  
677 Griswold JP (2004) Mobility statistics and hazard mapping for non-volcanic debris flows and rock avalanches. MS  
678 thesis, Portland State University  
679  
680 Hong Y, Wang JP, Li DQ et al. (2015) Statistical and probabilistic analyses of impact pressure and discharge of debris  
681 flow from 139 events during 1961 and 2000 at Jiangjia Ravine, China. *Engineering Geology* 187:122-134.  
682  
683 Hu K, Wei F, Li Y (2011) Real-time measurement and preliminary analysis of debris-flow impact force at Jiangjia  
684 Ravine, China. *Earth Surface Processes and Landforms*. 36:1268-1278.  
685  
686 Huebl J, Steinwendtner H (2000) Debris flow hazard assessment and risk mitigation. *Felsbau, Rock and Soil  
687 Engineering*, Vol.1, 17-23, Verlag Glueckauf (in German)  
688

689 Huebl J (2001) Strategy of protection. In: R. Didier and F. Zanolini (eds), Risques torrentiels. Université Européenne  
690 d'Été sur les Risques Naturels, Grenoble, France.

691

692 Huebl J, Holzinger G (2003) Kleinmassstäbliche Modellversuche zur Wirkung von Murbrechern. WLS Report 50,  
693 Institut für Alpine Naturgefahren, Wien. 3 pp. (in German).

694

695 Huebl J, Suda J, Proske D et al. G (2009) Debris Flow Impact Estimation. In Proceedings of 11th International  
696 Symposium on Water Management and Hydraulic Engineering (WMHE2009) Vol. 1:137-148.

697

698 Hungr O, Morgan GC, Kellerhals R (1984) Quantitative analysis of debris torrent hazard for design of remedial  
699 measures. *Can Geotech J* 21:663–667.

700

701 Hungr O (2005) Classification and terminology. In: *Debris flow Hazards and Related Phenomena*. Edited by M. Jakob  
702 and O. Hungr. Praxis Publishing Ltd., Chichester, UK 11-51.

703

704 Hungr O, Leroueil S, Picarelli L (2014) The Varnes classification of landslide types, an update. *Landslides* 11: 167-194.

705

706 Hutter K, Svendsen B, Rickenmann D (1994) Debris flow modeling: A review. *Continuum mechanics and*  
707 *thermodynamics* 8(1):1-35.

708

709 Iverson RM (1997) The physics of debris flows. *Rev Geophys* 35:245–296.

710

711 Iverson RM (2015) Scaling and design of landslide and debris-flow experiments. *Geomorphology* 244:9-20.

712

713 Jakob M, Hungr O (2005) *Debris-flow Hazards and Related Phenomena*. Springer-Verlag Berlin Heidelberg 445-487.

714

715 Jakob M, Holm K, McDougall S (2016) Debris-flow risk assessment. *Oxford Research Encyclopedias – Natural Hazard*  
716 *Science*. DOI: 10.1093/acrefore/9780199389407.013.37

717

718 Kienholz H (2003) Early warning systems related to mountain hazards. In: J. Zschau and A. Kueppers (eds), *Early*  
719 *Warning System for Natural Disaster Reduction: 3<sup>rd</sup> International IDNDR Conference on Early Warning System for the*  
720 *Reduction of Natural Disasters*. Postdam, 1998, 555-564, Springer-Verlag, Berlin.

721

722 Lamberti A, Zanuttigh B (2004) Experimental analysis of the impact of dry granular debris flows against obstacles.  
723 *XXIX Convegno di idraulica e costruzioni idrauliche*, Trento 571–578.

724

725 Leonardi A, Wittel FK, Mendoza M, Vetter R, Herrmann HJ (2016) Particle–fluid–structure interaction for debris flow  
726 impact on flexible barriers. *Computer-Aided Civil and Infrastructure Engineering* 31(5):323-333.

727

728 Lichtenhahn C (1973) Die Berechnung von Sperren in Beton und Eisen- beton, *Kolloquium on Torrent Dams*, Heft,  
729 *Mitteilungender Forstlichen Bundensanstalt Wien*. 91–127. (in German)

730  
731 Mizuyama T (2008) Structural countermeasures for debris flow disasters. *International Journal of Erosion Control*  
732 *Engineering* 1(2):38-43.  
733  
734 Moase EE (2017) Guidance for debris-flow and debris-flood mitigation design. Simon Fraser University. Master Thesis  
735  
736 Ng CWW, Song D, Choi CE, Koo CH, Kwan JSH (2016) A novel flexible barrier for landslide impact in centrifuge.  
737 *Géotechnique Lett* 6(3):221-225.  
738  
739 Ng CWW, Choi CE, Goodwin GR (2019) Froude characterization for single-surge unsteady dry granular flows: impact  
740 pressure and run up. *Can Geotech J* DOI: 10.1139/cgj-2018-0529.  
741  
742 Osanai N, Mizuno H, Mizuyama T (2010) Design Standard of Control Structures Against Debris Flow in Japan. *Journal*  
743 *of Disaster Research* 3(5):307-314.  
744  
745 Poudyal S, Choi CE, Song D et al. (2019) Review of mechanisms of debris-flow impact against barriers. In *Proceeding*  
746 *of the 7<sup>th</sup> International Conference on Debris-Flow Hazards Mitigations*, Colorado, USA 1027-1034.  
747  
748 Revellino P, Hungr O, Guadagno FM, Evans SG (2004) Velocity and runout simulation of destructive debris flows and  
749 debris avalanches in pyroclastic deposit, Campania region, Italy. *Environmental Geology* 45:295-311.  
750  
751 Santi PM, Hewitt K, VanDine DF, Barillas Cruz E (2011) Debris-flow impact, vulnerability, and response. *Nat Hazards*  
752 56(1): 371-402. DOI: 10.1007/s11069-010-9576-8  
753  
754 Scheidl C, Chiari M, Kaitna R, Mulleger M, Krawtschuk A, Zimmerman T, Proske D (2013) Analysing Debris Flow  
755 Impact Models, Based on a Small Scale Modelling Approach. *Surv Geophys* 34:121-140.  
756  
757 Scotton P, Deganutti AM (1997) Phreatic line and dynamic impact in laboratory debris flow experiments. In  
758 *Proceedings of the 1<sup>st</sup> ASCE International Conference on Debris-flow Hazard Mitigation: Mechanics, Prediction and*  
759 *Assessment*. San Francisco, USA 777–786.  
760  
761 Shen W, Zhao T, Zhao J, Dai F, Zhou G (2018) Quantifying the impact of dry debris flow against a rigid barrier by  
762 DEM analyses. *Engineering Geology* 241:86-96.  
763  
764 Song D, Choi CE, Ng CWW, Zhou GGD (2017) Geophysical flows impacting a flexible barrier: effects of solid-fluid  
765 Interaction. *Landslides* 15(1):99-110.  
766  
767 Sovilla B, Faug T, Kohler A, Baroudi D, Fischer J, Thibert E (2016) Gravitational wet avalanche pressure on pylon-like  
768 structures. *Cold Regions Science and Technology* 126:66–75.  
769

770 Suda J, Huebl J, Bergmeister K (2010) Design and construction of high stressed concrete structures as protection works  
771 for torrent control in the Austrian Alps. In Proceedings of 3<sup>rd</sup> fib international Congress, Washington, USA, 1-12.  
772

773 Suwa H, Okuda S (1983) Deposition of debris flows on a fan surface, Mt. Yakedake, Japan. *Zeitschrift Geomorph N F*  
774 *Suppl Bd* 46:79–101.  
775

776 Takahashi T (2007) *Debris Flow. Mechanics, Prediction and Countermeasures*. Taylor and Francis Group.  
777

778 Turnbull B, Bowman ET, McElwaine JN (2015) Debris flow: experiments and modelling. *Comptes rendus physique*  
779 16:86-96.  
780

781 Vagnon F, Ferrero AM, Segalini A (2016) EC7 design approach for debris flow flexible barriers: applicability and  
782 limitations. In: Gercek H., Ulusay R., Hindistan M.A., Tuncay E., Aydan O. (eds), *Mechanics and Rock Engineering:*  
783 *From the Past to the Future*. International Symposium on International Society for Rock Mechanics, ISRM 2016.  
784 Cappadocia, Turkey, 29-31 August 2016, 1, 499-504, CRC Press/Balkema.  
785

786 Vagnon F, Segalini A (2016) Debris flow impact estimation on a rigid barrier. *Nat Hazards Earth Syst Sci* 16:1691–  
787 1697. doi:10.5194/nhess-16-1691-2016.  
788

789 Vagnon F, Ferrero AM, Umili G, Segalini A (2017a) A Factor Strength Approach for the Design of Rock Fall and  
790 Debris Flow Barriers. *Geotech Geol Eng* 35(6):2663-2675.  
791

792 Vagnon F, Ferrero AM, Latham JP, Xiang J (2017b) Benchmarking of debris flow experimental tests using combined  
793 finite-discrete element method, FEMDEM. In Proceedings of ISRM Afrirock – Rock Mechanics for Africa, 739-752.  
794

795 VanDine DF (1996) Debris flow control structures for forest engineering. Research Branch, BC Ministry of Forests,  
796 Victoria, BC. Working paper 08/1996. 75 pages.  
797

798 Watanabe M, Ikeya H (1981) Investigation and analysis of volcanic mud flows on Mount Sakurajima, Japan. Erosion  
799 sediment transport measurement. In: *Int Assoc Hydrol Sei Publ*, 133, Florence, 245–256.  
800

801 Wendeler C, Volkwein A (2015) Laboratory tests for the optimization of mesh size for flexible debris-flow barriers, *Nat*  
802 *Hazards Earth Syst Sci* 15:2597-2604. DOI:10.5194/nhess-15-2597-2015.  
803

804 Wendeler C, Volkwein A, McArdeall BW, Bartelt P (2018) Load model for designing flexible steel barriers for debris  
805 flow mitigation. *Canadian Geotechnical Journal* 99:1-39.  
806

807 Zanchetta G, Sulpizio R, Pareschi M, Leoni F, Santacroce R (2004) Characteristics of May 5-6, 1998 volcanoclastic  
808 debris flows in the Sarno area (Campania, southern Italy): Relationships to structural damage and hazard zonation.  
809 *Journal of volcanology and geothermal research* 133:377-393.  
810

- 811 Zhang S (1993) A comprehensive approach to the observation and prevention of debris flows in China. *Nat Hazards*  
812 7:1–23.  
813
- 814 Zimmerman M, Haeberli W (1992) Climatic change and debris flow activity in high mountains areas. A case study in  
815 the Swiss Alps. *Catena Suppl* 22:59–72.  
816

817 **List of Figures**

818 **Fig. 1** Different types of debris flow active mitigation measures: check dam (photograph by Los Angeles County Flood  
819 Control District) (a), open type sabo structures (photograph of steel check dam in Nagano prefecture, Japan) (b),  
820 concrete slit barrier (photograph by LCW Consult web site of protection works in St. Luzia River, Madeira, Portugal)  
821 (c) and flexible net barrier (photograph by Geovertical S.R.L web site of protection works in Terranova Pollino,  
822 Basilicata Region, Italy) (d).

823

824 **Fig. 2** Comparison between normalized debris flow impact force and hydro-static predicting models as function of  
825 Froude number considering small- (a) and full-scale experiments (b) and field data (c).

826

827 **Fig. 3** Relationship between measured peak pressure and calculated hydro-static peak pressure with  $k$  respectively equal  
828 to 2.5 (a to c) and 7.5 (d to f) as a function of the Froude number considering both small- (a, d) and full- scale (b, e) and  
829 field dataset (c, f). The green continuous line represents the perfect correspondence between measured values and  
830 estimated ones.

831

832 **Fig. 4** Comparison between normalized debris flow impact force and hydro-dynamic predicting models as function of  
833 Froude number considering small- (a) and full-scale tests (b) as well as field data (c).

834

835 **Fig. 5** Relationship between measured peak pressure and calculated hydro-dynamic peak pressure with  $\alpha$  respectively  
836 equal to 0.4 (a to c) and 12 (c to d) as a function of the Froude number considering both small- (a, d) and full-scale (b,  
837 e) and field dataset (c, f)..

838

839 **Fig. 6** Relationship between velocity (blue squares) and thickness (red diamonds) as function of Froude number for  
840 small-scale tests (a) and full-scale and field data (b). A negative correlation exists between velocity and thickness: when  
841 Froude number increases, velocity increases and consequently flow height decreases and vice-versa.

842

843 **Fig. 7** Comparison between normalized debris flow impact force and mixed predicting models as function of Froude  
844 number considering small- (a) and full-scale test (b) as well as field data (c).

845

846 **Fig. 8** Relationship between measured peak pressure and calculated peak pressure for different mixed models as a  
847 function of the Froude number considering field dataset (a to f).

848

849 **Fig. 9** Predicting capability analysis of hydro-static models using field dataset.

850

851 **Fig. 10** Predicting capability analysis of hydro-dynamic models using field dataset.

852

853 **Fig. 11** Predicting capability analysis of mixed models using field dataset.

854

855 **Fig. 12** Relationship between field measurements of the peak pressure and calculated peak pressure using hydro-static  
856 formulation with  $k=1$  as a function of the Froude number of the flow

857

858 **Fig. 13** Relationship between peak pressure ratio for the modified hydro-static model as a function of the Froude  
859 number (a) and statistical evaluation of the predicting capability of the proposed model (b).

860

861 **Fig. 14** Comparison between the proposed model (black line) and others hydro-dynamic (Hungar et al. 1984 and Canelli  
862 et al. 2012) and mixed (Arattano and Franzini 2003, Huebl and Holzinger 2003, Lamberti and Zanuttigh 2004, Armanini  
863 et al. 2011, Cui et al. 2015 and Vagnon and Segalini 2016) models.

864

Author	Coefficient	Data source	Notes
Lichtenhahn (1973)	3.5 – 5.5	Theoretical and construction experience	Hydro-static formula
Armanini (1997)	4.5	Theoretical and laboratory experiments	Hydro-static formula
Scotton and Deganutti (1997)	2.5 – 7.5	Laboratory experiments	Hydro-static formula
Watanabe and Ikeya (1981)	2.0 – 4.0	Field measurements of volcanic mud flows	Hydro-dynamic model
Daido (1993)	5 – 12	Analytical results	Hydro-dynamic model
Bugnion et al. (2011)	0.4 – 0.8	Measurements of generated hillslope debris flow at Canton Aargau, Switzerland	Hydro-dynamic model
Canelli et al. (2012)	1.5 – 5.5	Laboratory experiments and field measurements	Hydro-dynamic model
Hungr et al. (1984)	1.5	Back-analysis data in British Columbia, Canada	Hydro-dynamic model
Zhang (1993)	3.0 – 5.0	Field measured data in Jiangjia ravine, China	Hydro-dynamic model
Huebl and Holzinger (2003)	5	Field and laboratory experimental data	Mixed model
Cui et al. (2015)	5.3	Field and laboratory experimental data	Mixed model
Cross (1967)	$k = 0.5$ $\alpha = 3$	Tsunami wave pressure	Mixed model
Arattano and Franzi (2003)	1	Field measured data in Moscardo Torrent, Italy	Mixed model
Lamberti and Zanuttigh (2004)	1.5	Theoretical and laboratory experiments	Mixed model
Armanini et al. (2011)	1	Theoretical and laboratory experiments	Mixed model
Vagnon and Segalini (2016)	0.5 – 1.2	Theoretical and laboratory experiments	Mixed model

**Table 2 – Summary of the main dataset characteristics.**

	Dataset	Apparatus/Basin	Material	Measured Physical Quantities	Dimension of the dataset
Small-scale experiments	Scheidl et al. 2013	Wood flume with constant inclination of 30° and measuring section 4.5 m long and 0.45 m wide. The reservoir section can release a volume equals to 0.33 m <sup>3</sup> of mixture.	Mixture with constant dry mass and variable water content (from 0.16 to 0.27). The grain size distribution ranges between 0.0002 and 50 mm	Flow velocity, impacting height and horizontal impact forces recorded in real time during the experiments.	30 experiments but only 16 selected for further analyses
	Cui et al. 2015	Steel flume 0.2 m wide and 3 m long with slope ranging from 10° to 15°.	Material collected in the Jiangjia Ravine basin (China) with grain size distribution varying between 0.001 and 10 mm. The liquid concentration varies from 0.34 to 0.76.	Flow velocity, impacting height and pressure recorded in real time during the experiments.	27 tests with different density (1600-2300 kg m <sup>-3</sup> ) and slopes (10-13°).
	Ashwood and Hungr 2016	Steel flume 0.3 m wide and 3 m long with slope ranging from 22° to 34°.	Uniform quartz sand and pea gravel	Flow velocity, impacting height, profile, barrier deflection and pressure recorded in real time during the experiments.	28 tests with different density (1560-1780 kg m <sup>-3</sup> ) and slopes (122-34°).
	Vagnon and Segalini 2016	Steel flume 4 m long and 0.39 m wide in which the slope is variable between 30° and 35°	Saturated sand with constant liquid concentration (0.4) and mixture density (1920 kg m <sup>-3</sup> ). The grain size distribution varies between 0.0001 and 5 mm.	Flow velocity, impacting height and impact forces recorded in real time during the experiments.	63 test with different volume released and different slopes.
Full-scale experiments	DeNatale et al. 1999	A 41m long, 8m wide channel constructed on the side of a rock quarry near Velthein, Switzerland. Average inclination of 30°	Mixture of soil, bedrock and water	Flow height at the middle of channel, velocity of upper flow surface, impact pressure on two different steel plates	16 tests with single or multiple releases. Density varies between 1760 and 2110 kg/m <sup>3</sup>
	Bugnion et al. 2011	USGS debris flow flume, 95m long, 2m wide and 1.2 deep, with constant slope of 31°	Poorly graded, clean and saturated gravelly sand	Flow height, velocity, impact pressure on flexible barrier	6 experiments on flexible barriers
Field measurements	Wendeler et al. 2007	Barrier system installed at the Illgraben basin, Switzerland	Muddy debris flow	Flow height, load cells, velocity from video record	May 18th 2006 event
	Hu et al. 2011	Jiangjia Ravine basin, located near the city of Dongchuan (China). the basin has an area of 48.6 km <sup>2</sup> and the mainstream has a length of 13.9 km.	The bulk density ranges from 1600 to 2300 kgm <sup>-3</sup> with fluid concentration ranging from 0.15 to 0.6. The dimension of the solid particles varies between 0.001 and	Flow velocity, impacting height and impact forces recorded in real time during debris flow events.	38 surges occurred on August 25, 2004 after short intense rainfall

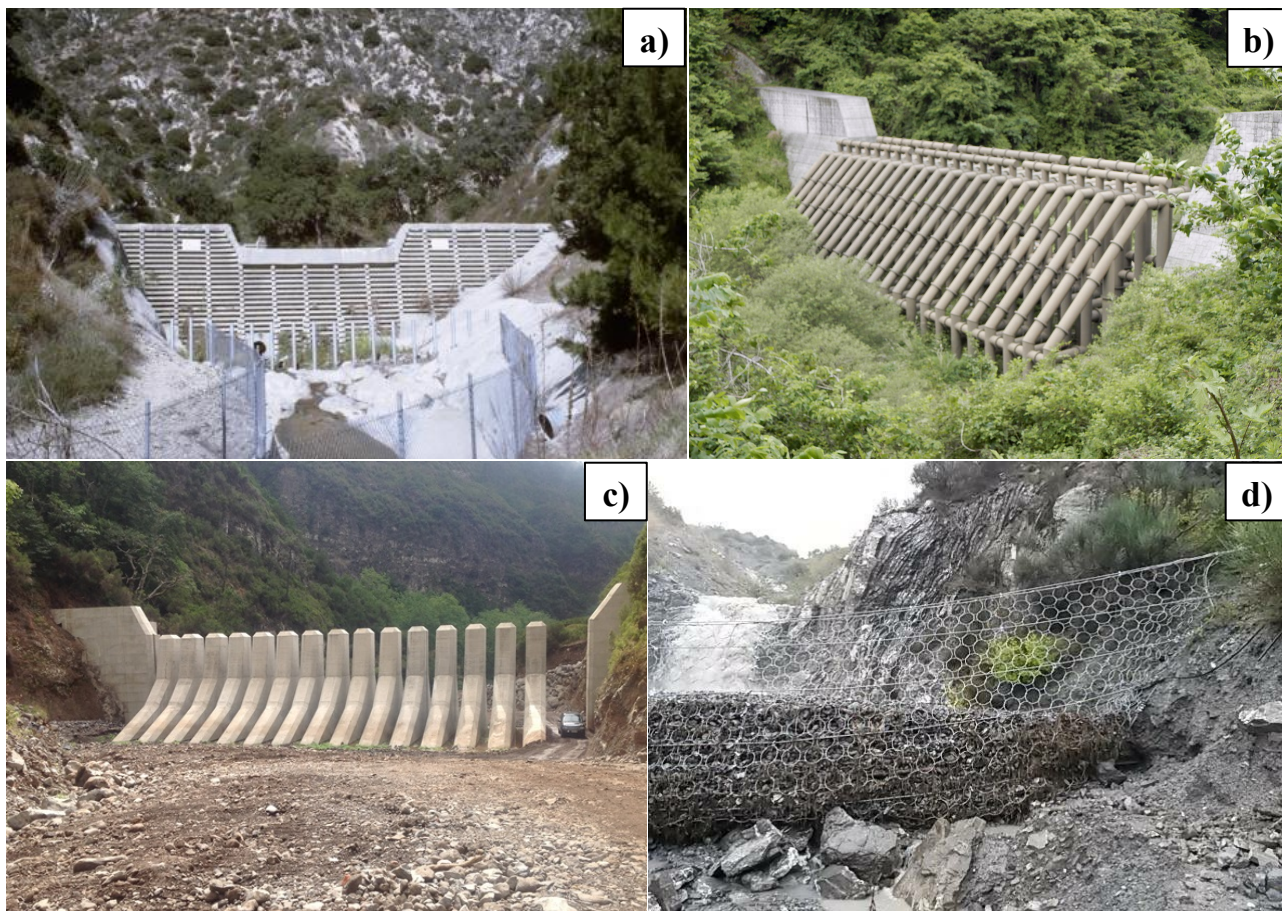
100 mm.

Hong et al. 2015	Jiangjia Ravine basin, located near the city of Dongchuan (China). the basin has an area of 48.6 km <sup>2</sup> and the mainstream has a length of 13.9 km.	The bulk density ranges from 1600 to 2300 kgm <sup>-3</sup> with fluid concentration ranging from 0.15 to 0.6. The dimension of the solid particles varies between 0.001 and 100 mm.	Channel width, flow velocity, impacting height, density, duration and impact forces recorded in real time during debris flow events.	139 events during 1961 and 2000
McArdell 2016	Illgraben basin, Switzerland	Quartzite and dolomite boulders, clast-size particles	Flow height, load cells, velocity from video record	29 July, 8 August and 24 August 2013 events

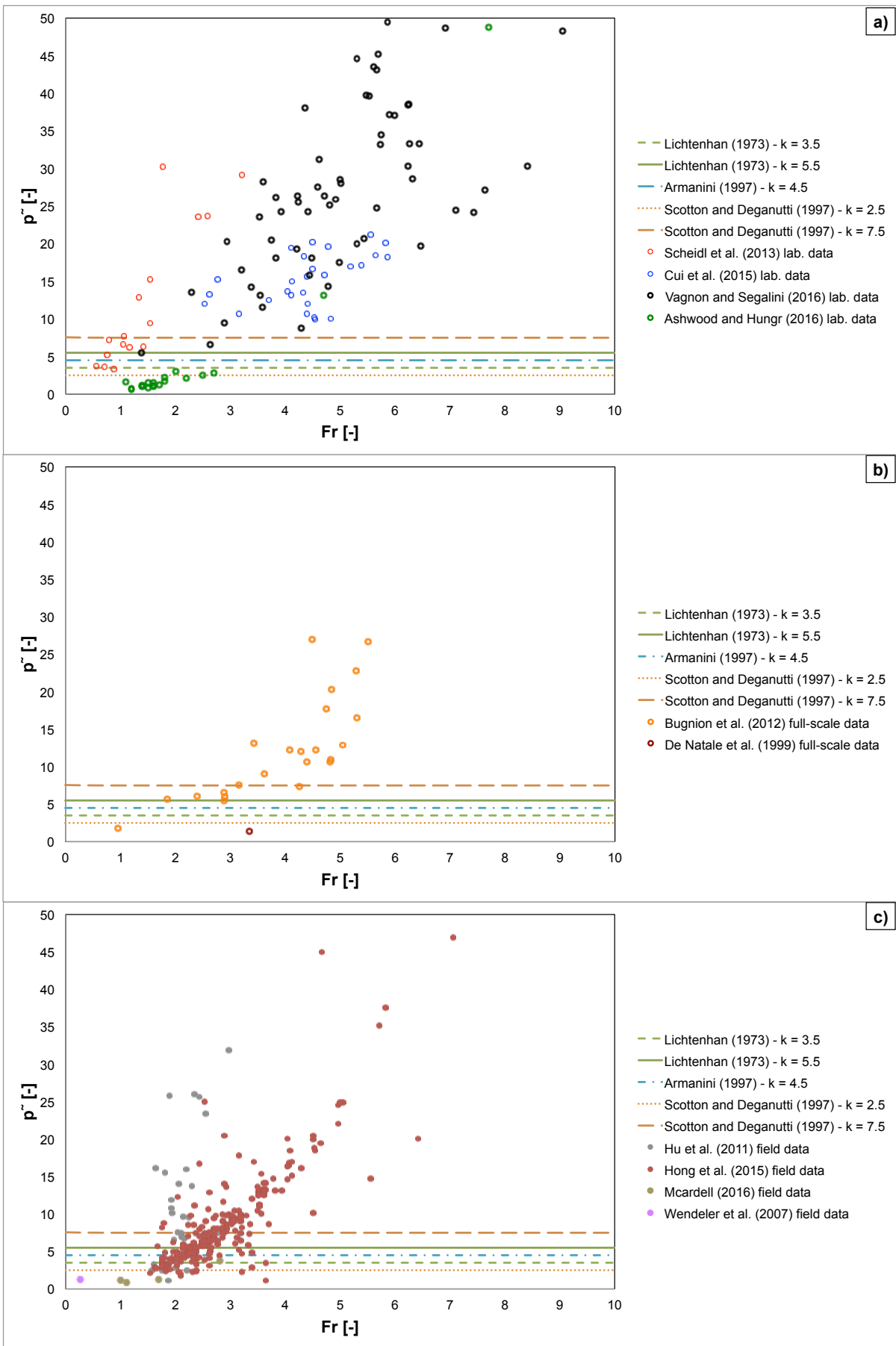
---

**Table 3 – Evaluation of the peak pressure prediction capability for debris flow impact models.**

Model type	Equation	Empirical coefficient [-]	Percentage of overestimated peak pressure values [%]		
			Small-scale dataset	Full-scale dataset	Field measurement
Hydro-static models	Lichtenhan (1973)	3.5	14.2	8.3	14.6
		5.5	17.2	12.5	35.6
	Armanini (1993)	4.5	15.7	8.3	25.4
	Scotton and Deganutti (1997)	2.5	11.2	8.3	5.4
		7.5	20.9	33.3	54.7
Hydro-dynamic models	Watanabe and Ike (1981)	2	82.1	100	91.2
		4	91	100	97.6
	Hungr et al. (1984)	1.5	72.4	91.7	86.1
	Daido (1992)	5	93.3	100	99
		12	100	100	98.7
	Zang (1993)	3	88.1	100	95.3
		5	93.3	100	99
	Bugnion et al. (2011)	0.4	0	4.2	2
		0.8	34.33	66.7	16.9
	Canelli et al. (2012)	1.5	72.4	91.7	86.1
		5.5	93.3	100	99
Mixed models	Cross (1967)	$k = 1; \alpha = 3$	88.1	100	94.3
	Arattano and Franzi (2003)	1	48.5	83.3	66.8
	Huebl and Holzinger (2003)		38.1	79.2	80.9
	Lamberti and Zanuttigh (2004)		64.2	100	87.9
	Armanini et al. (2011)	1	70.1	91.7	76.8
	Cui et al. (2015)		20.9	54.2	65.4
	Vagnon and Segalini (2016)	1.2	85.1	87.5	84.6
Number of small-scale tests			134		
Number of small-scale tests			24		
Number of field measurements			298		



874  
875 **Fig. 1** Different types of debris flow active mitigation measures: check dam (photograph by Los Angeles County Flood  
876 Control Distric) (a), open type sabo structures (photograph of steel check dam in Nagano prefecture, Japan) (b),  
877 concrete slit barrier (photograph by LCW Consult web site of protection works in St. Luzia River, Madeira, Portugal)  
878 (c) and flexible net barrier (photograph by Geovertical S.R.L web site of protection works in Terranova Pollino,  
879 Basilicata Region, Italy) (d).  
880

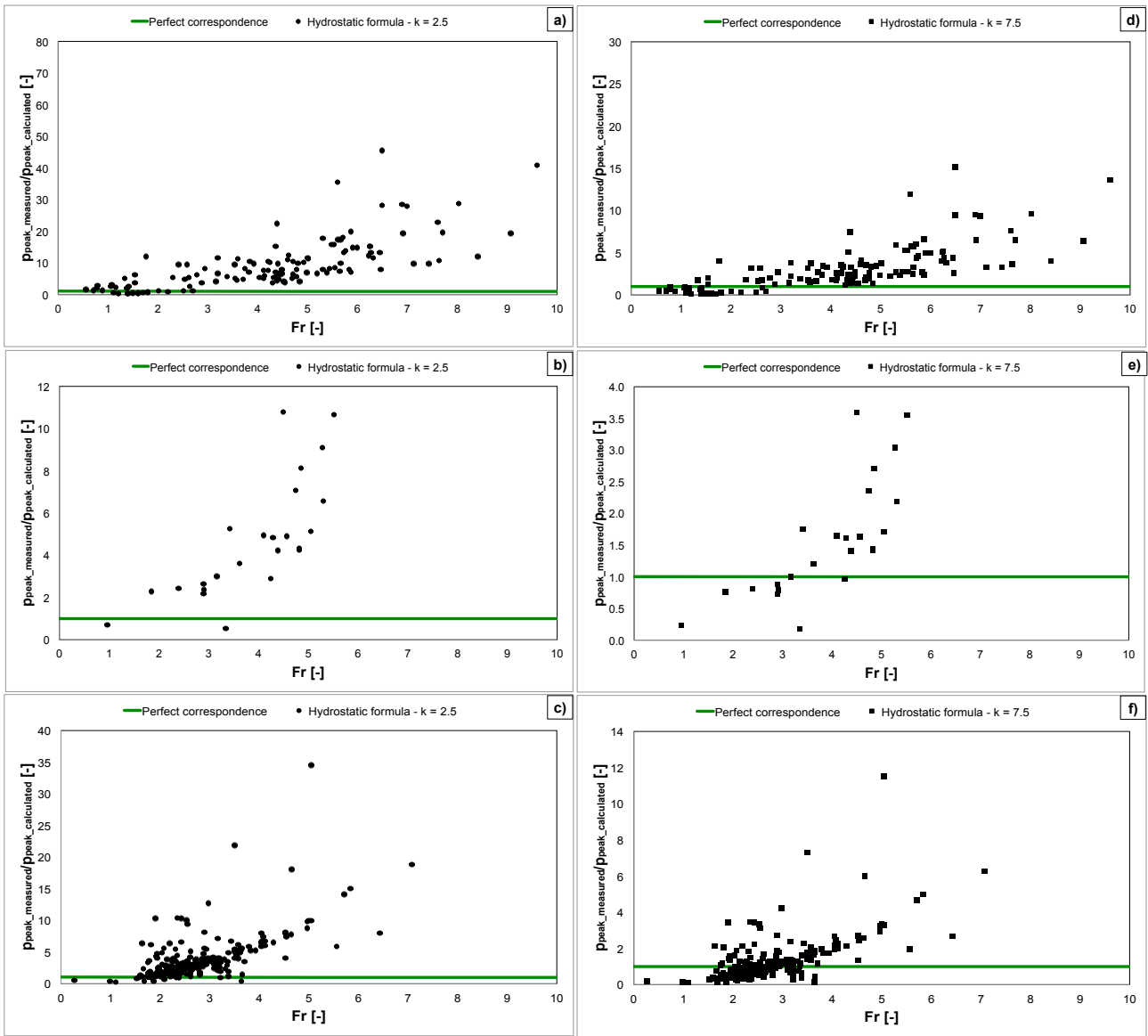


881

882

883

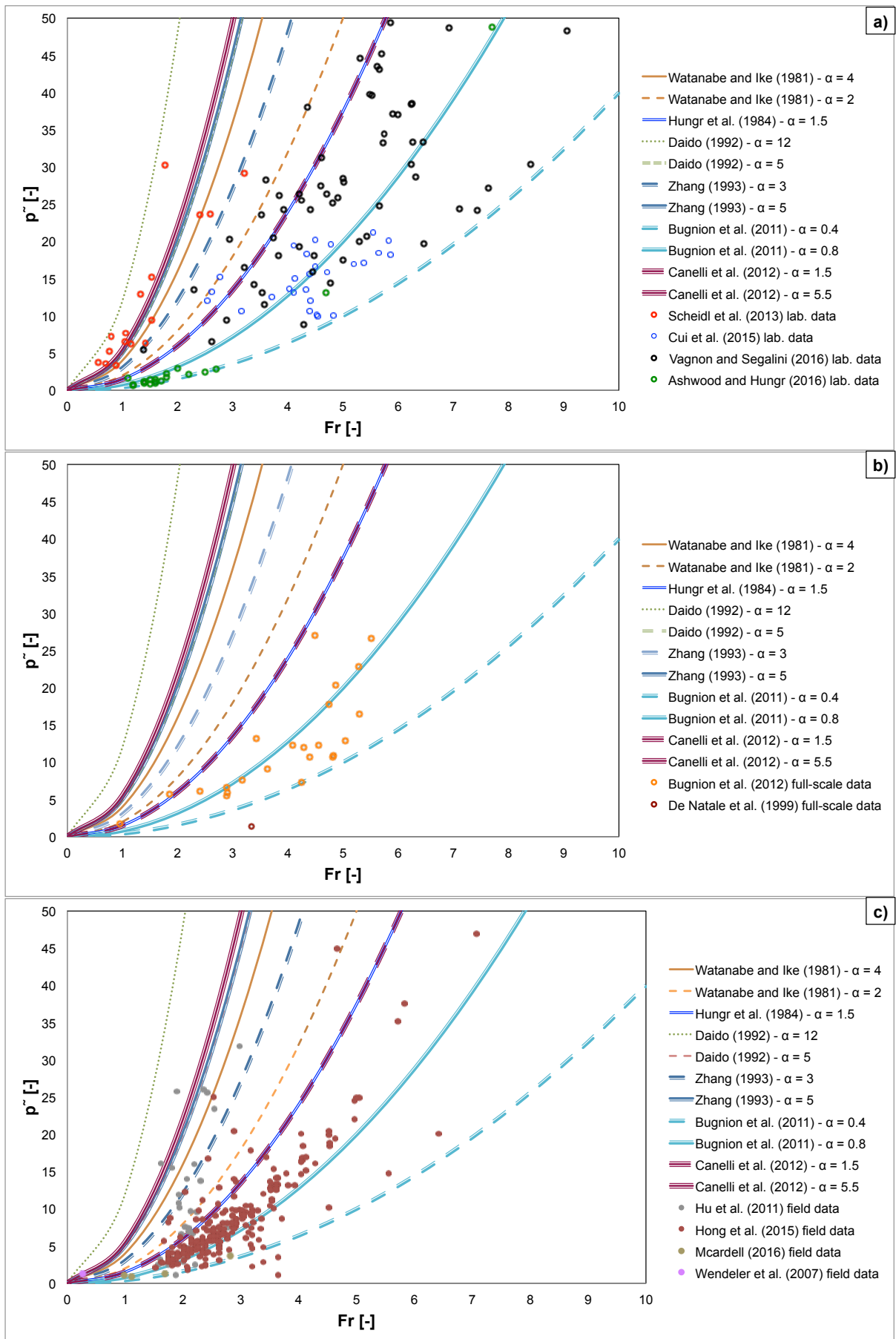
**Fig. 2** Comparison between normalized debris flow impact force and hydro-static predicting models as function of Froude number considering small- (a) and full-scale experiments (b) and field data (c).



884

885 **Fig. 3** Relationship between measured peak pressure and calculated hydro-static peak pressure with  $k$  respectively equal  
 886 to 2.5 (a, to c) and 7.5 (d to f) as a function of the Froude number considering both small- (a, d) and full- scale (b, e) and  
 887 field dataset (c, f). The green continuous line represents the perfect correspondence between measured values and  
 888 estimated ones.

889

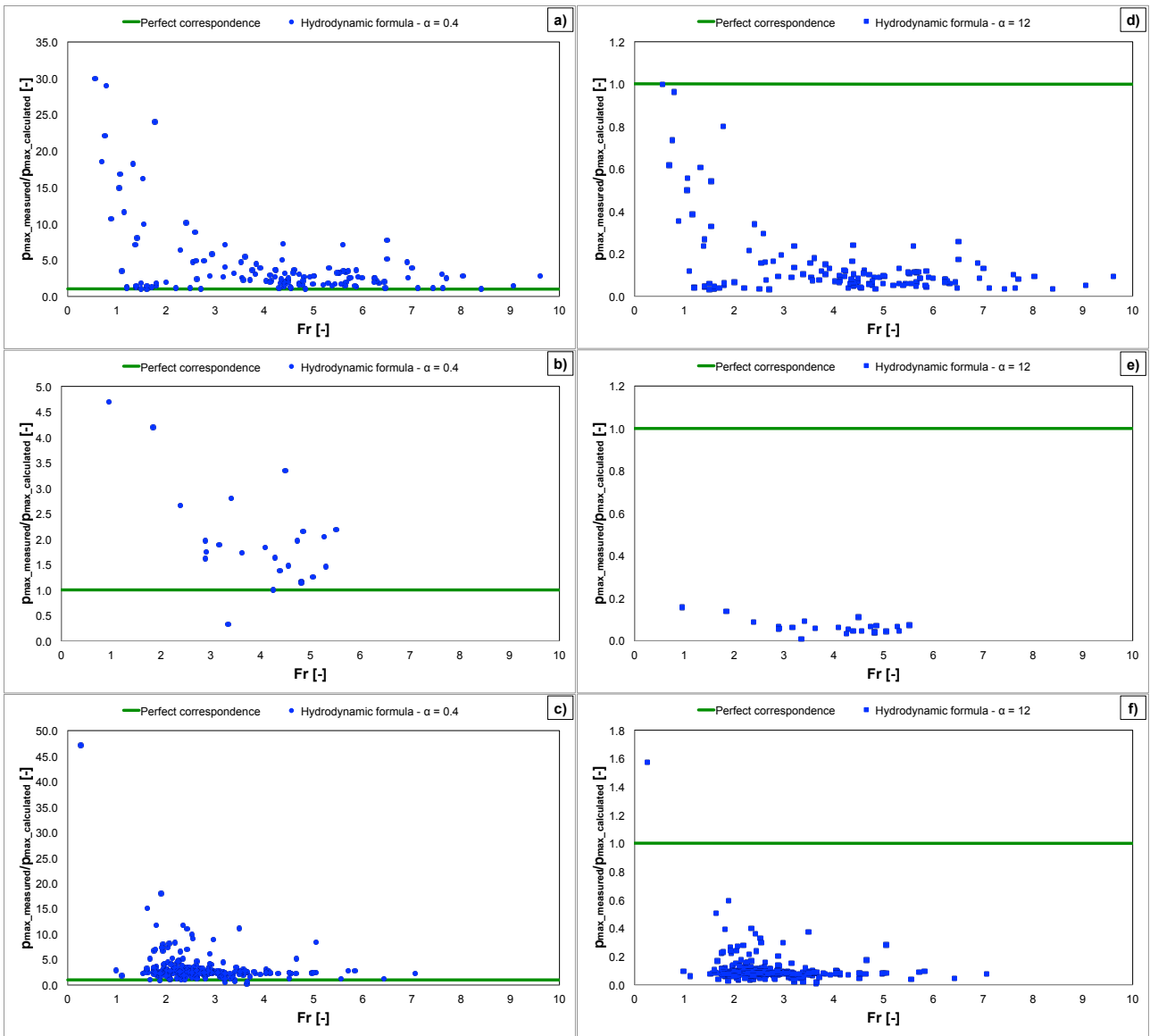


890

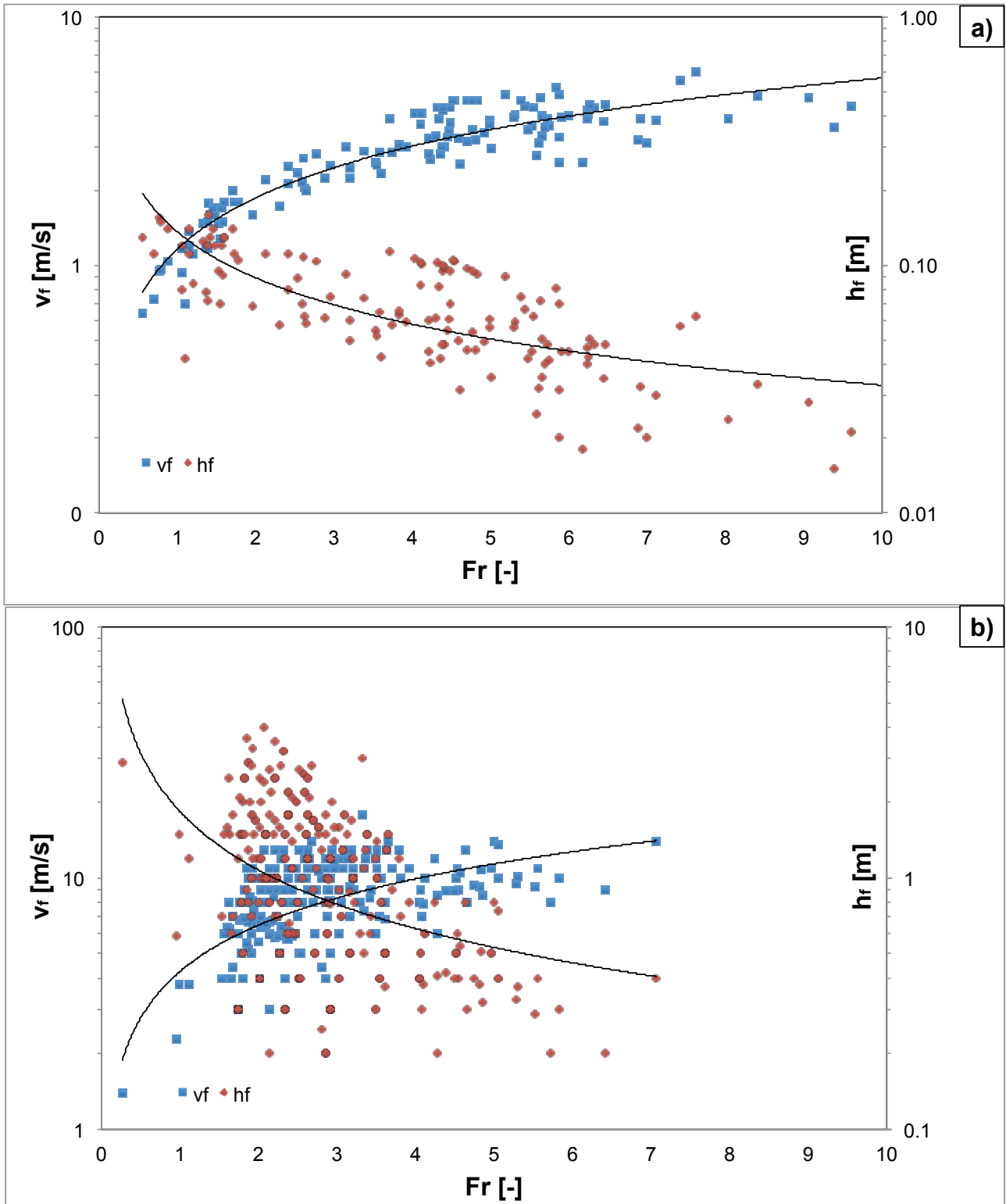
891

892

**Fig. 4** Comparison between normalized debris flow impact force and hydro-dynamic predicting models as function of Froude number considering small- (a) and full-scale tests (b) as well as field data (c).



893  
 894 **Fig. 5** Relationship between measured peak pressure and calculated hydro-dynamic peak pressure with  $\alpha$  respectively  
 895 equal to 0.4 (a to c) and 12 (c to d) as a function of the Froude number considering both small- (a, d) and full-scale (b,  
 896 e) and field dataset (c, f).  
 897



898

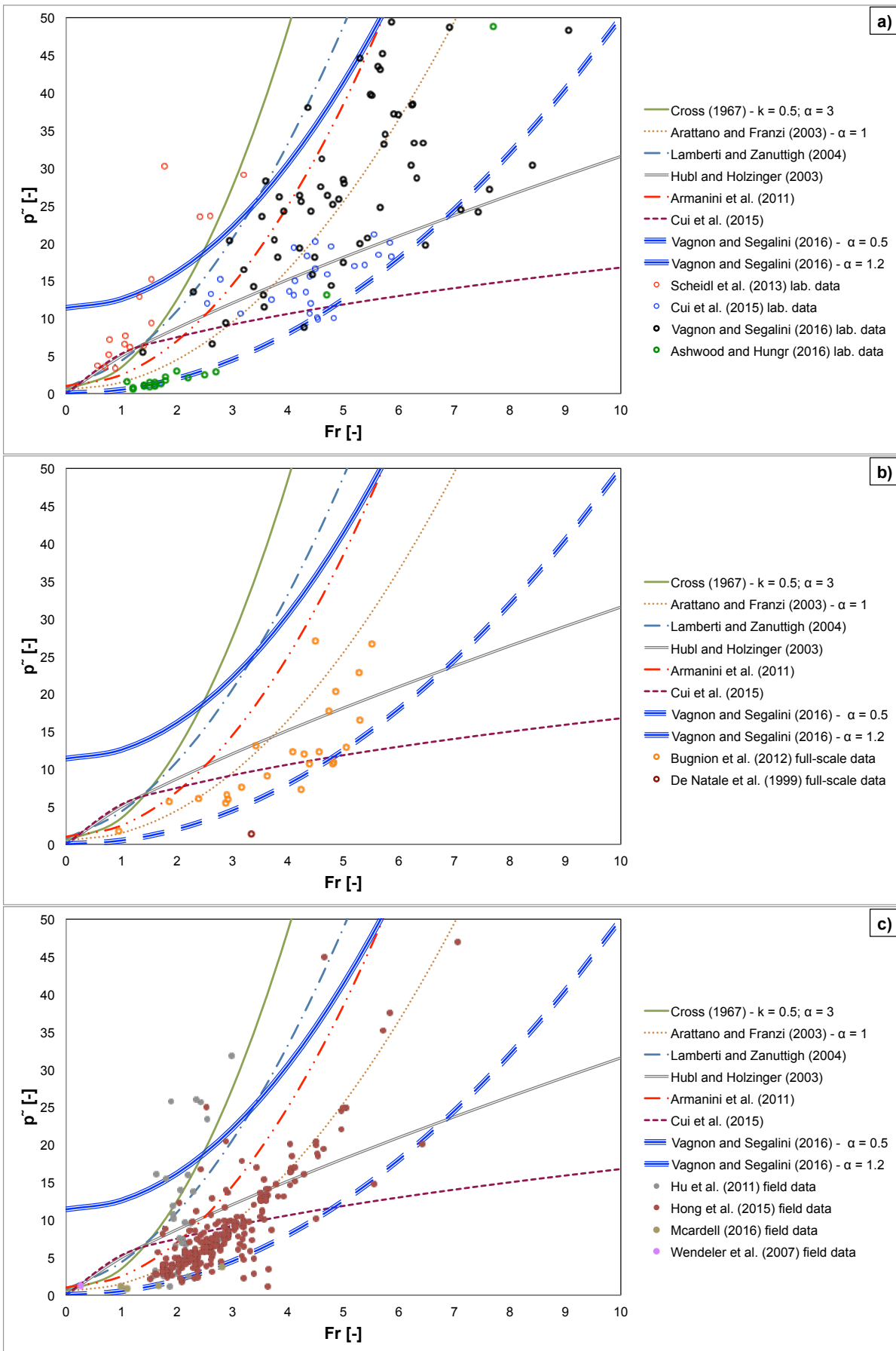
899

900

901

902

**Fig. 6** Relationship between velocity (blue squares) and thickness (red diamonds) as function of Froude number for small-scale tests (a) and full-scale and field data (b). A negative correlation exists between velocity and thickness: when Froude number increases, velocity increases and consequently flow height decreases and vice-versa.

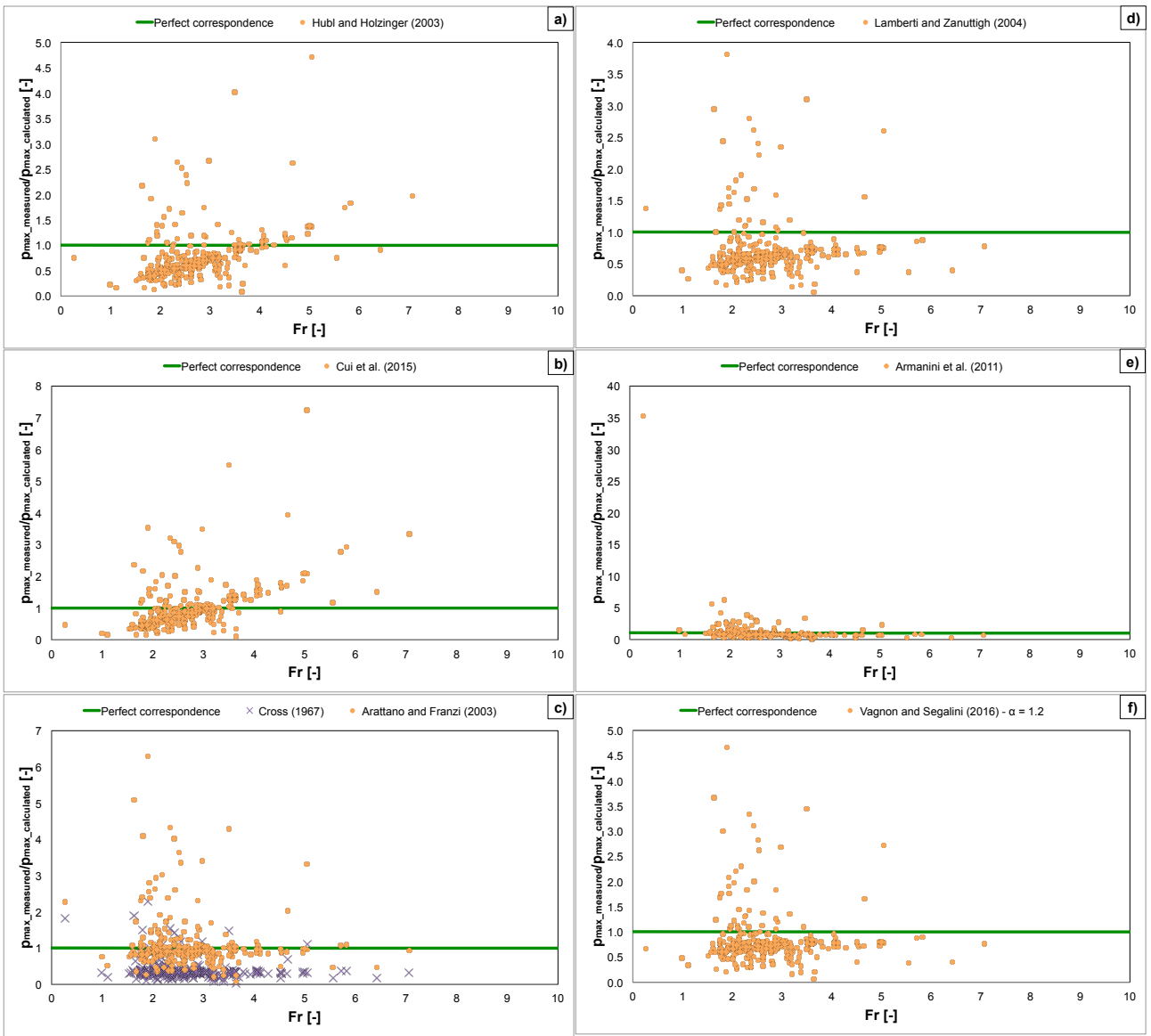


903

904

905

**Fig. 7** Comparison between normalized debris flow impact force and mixed predicting models as function of Froude number considering small- (a) and full-scale test (b) as well as field data (c).



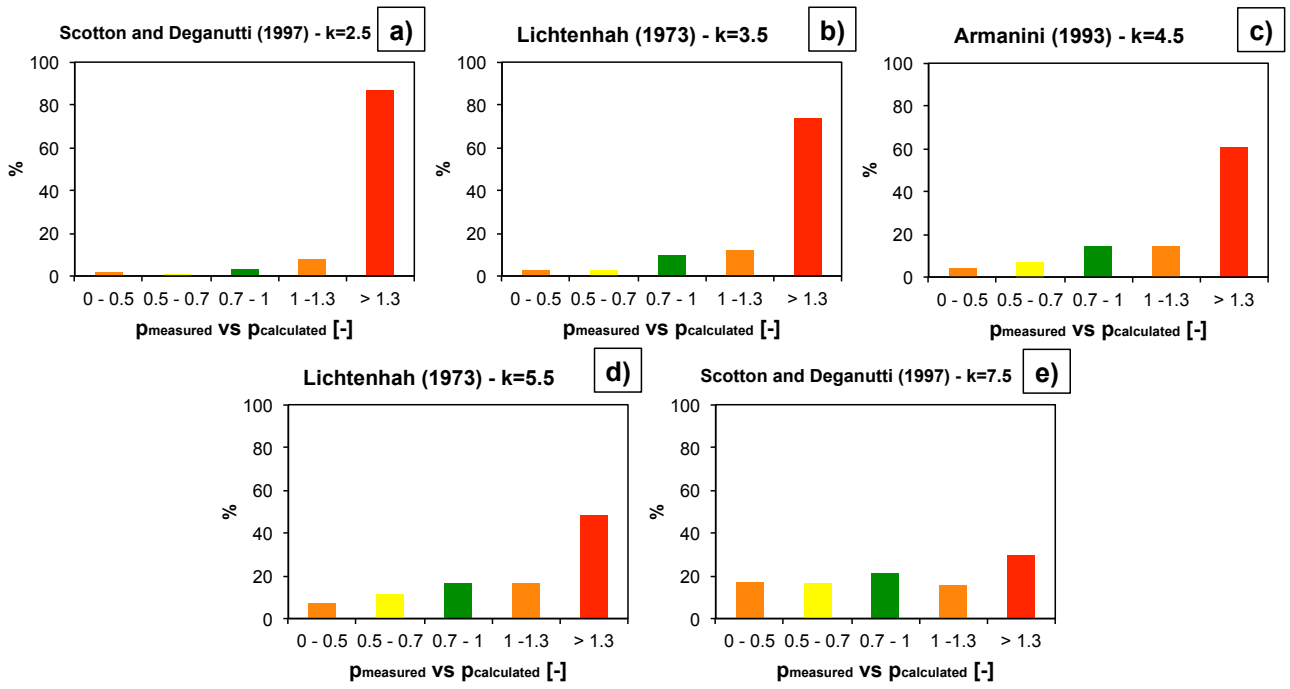
906

907

**Fig. 8** Relationship between measured peak pressure and calculated peak pressure for different mixed models as a function of the Froude number considering field dataset (a to f).

908

909

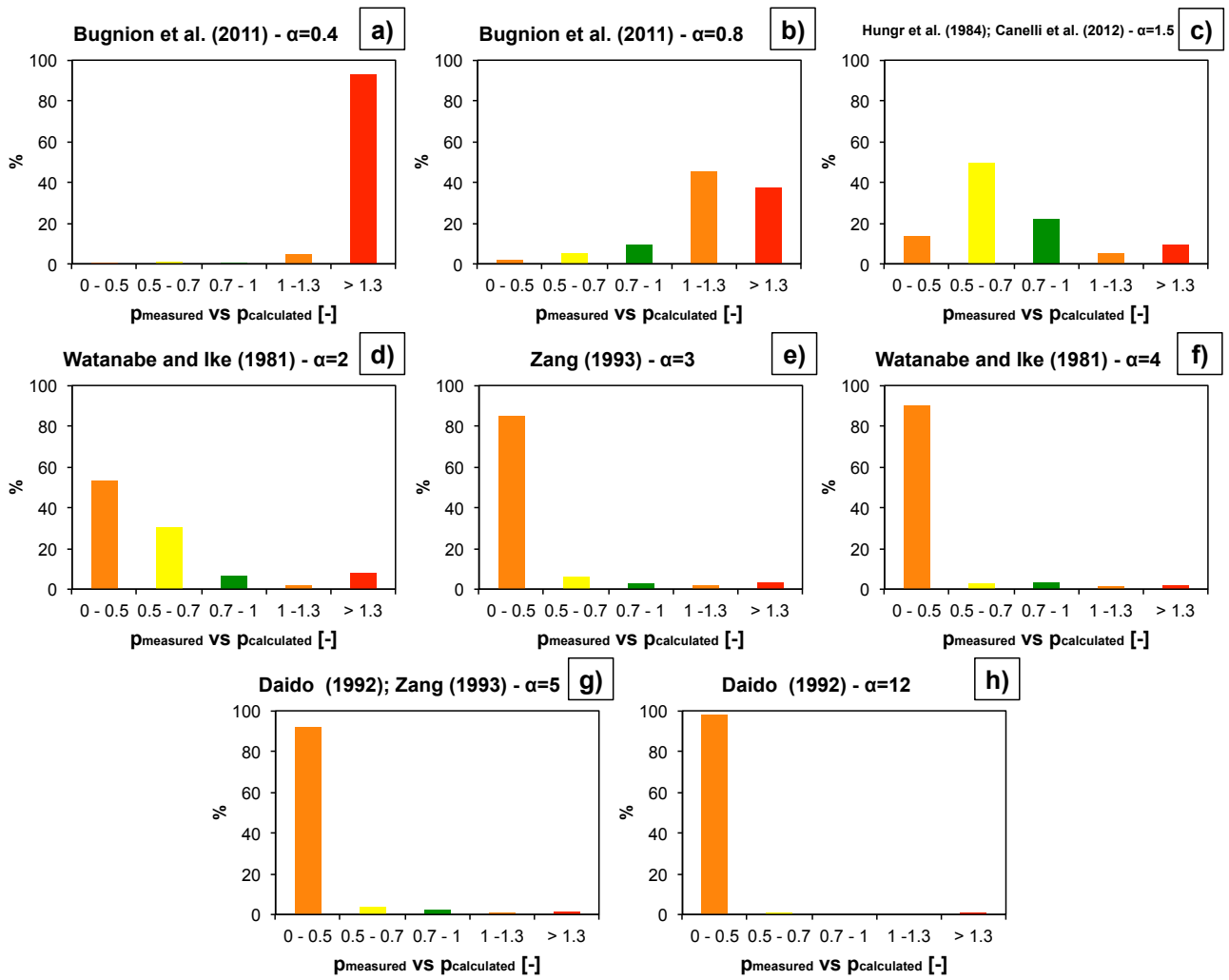


910

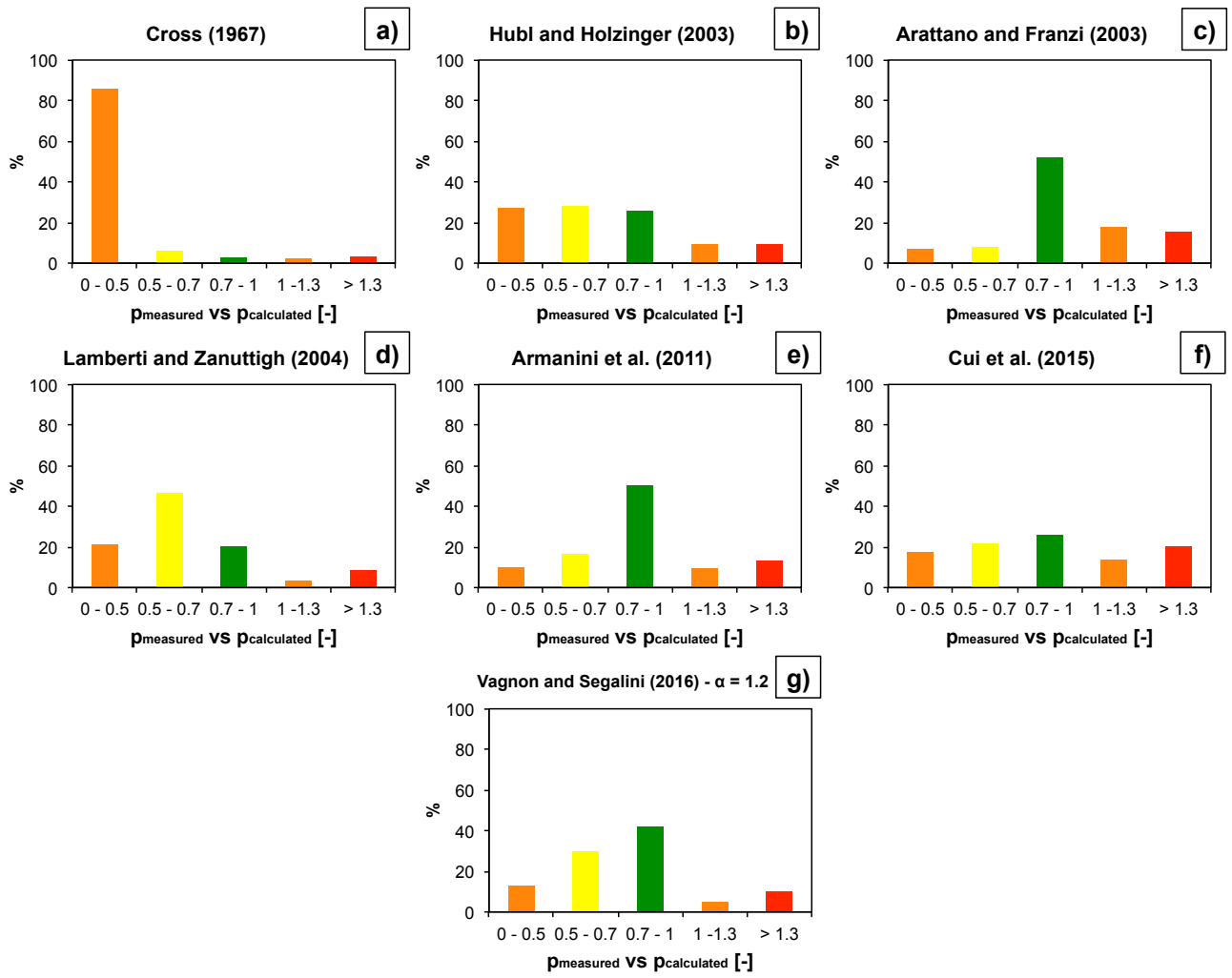
911

**Fig. 9** Predicting capability analysis of hydro-static models using field dataset.

912



913  
 914 **Fig. 10** Predicting capability analysis of hydro-dynamic models using field dataset.  
 915

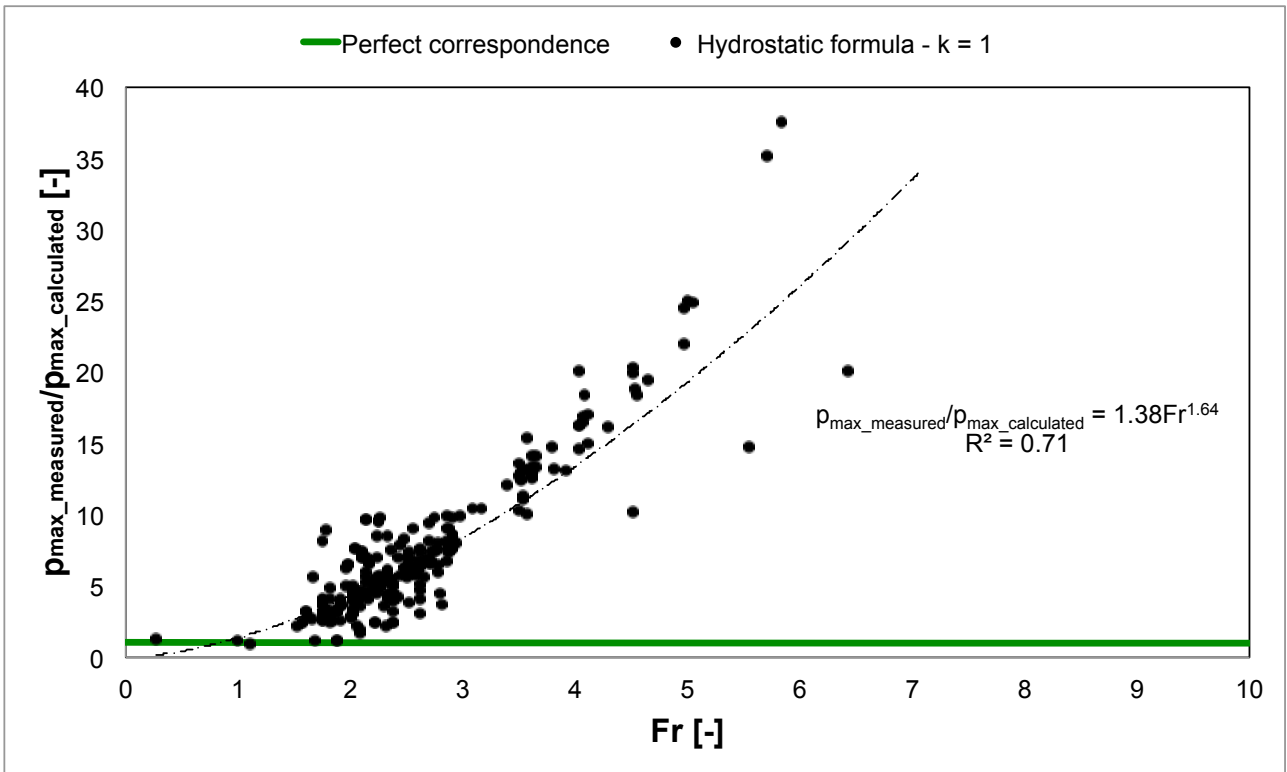


916

917 **Fig. 11** Predicting capability analysis of mixed models using field dataset.

918

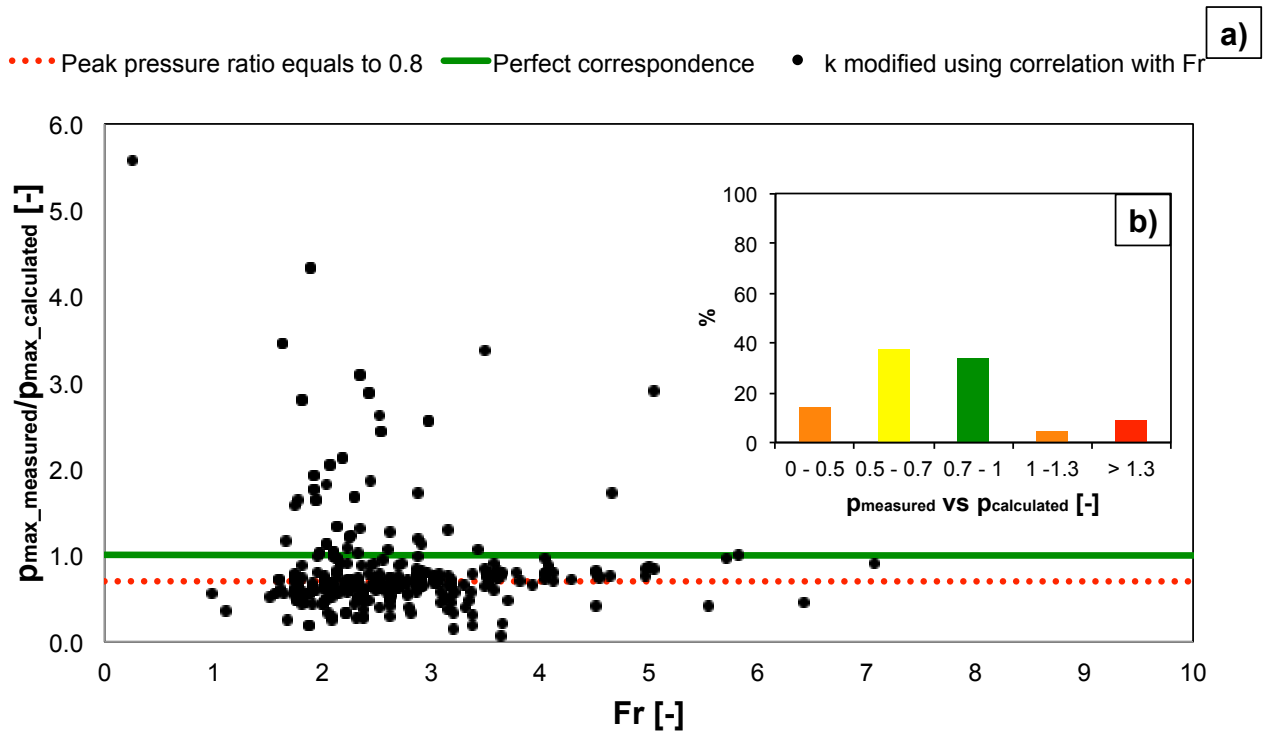
919



920

921 **Fig. 12** Relationship between field measurements of the peak pressure and calculated peak pressure using hydro-static  
 922 formulation with  $k=1$  as a function of the Froude number of the flow.

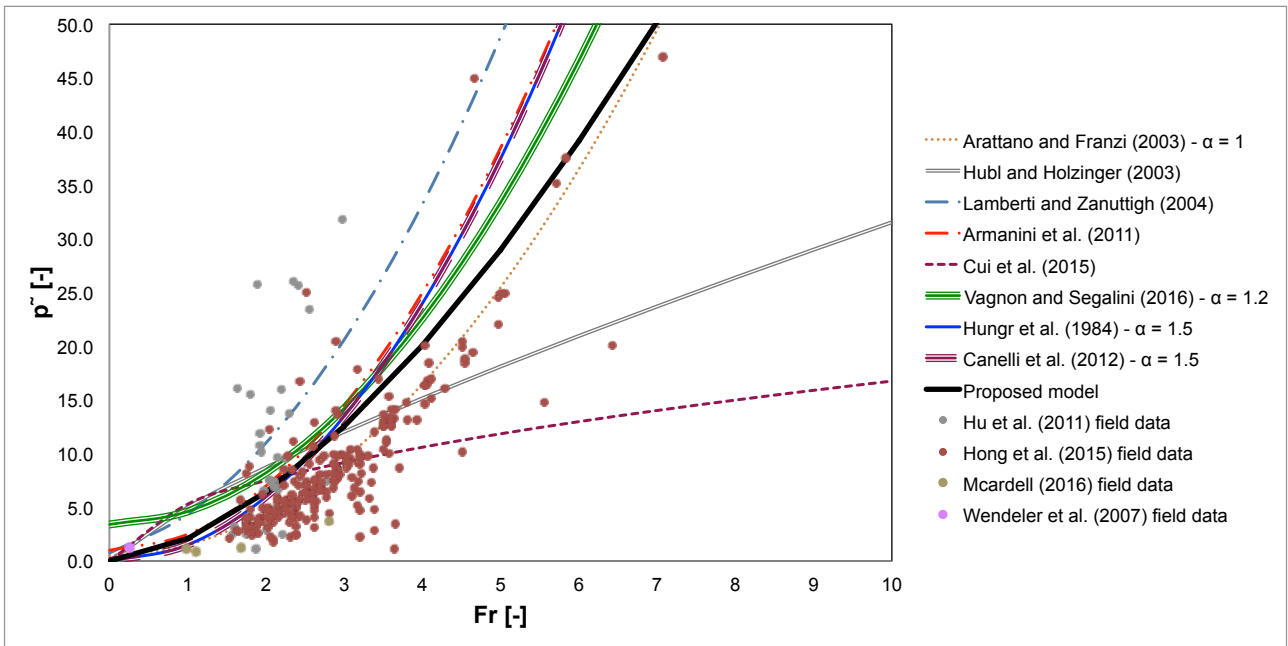
923



924

925 **Fig. 13** Relationship between peak pressure ratio for the modified hydro-static model as a function of the Froude  
 926 number (a) and statistical evaluation of the predicting capability of the proposed model (b).

927



928

929

930

931

**Fig. 14** Comparison between the proposed model (black line) and others hydro-dynamic (Hungr et al. 1984 and Canelli et al. 2012) and mixed (Arattano and Franzì 2003, Huebl and Holzinger 2003, Lamberti and Zanuttigh 2004, Armanini et al. 2011, Cui et al. 2015 and Vagnon and Segalini 2016) models.